SHOCK ATTENUATION IN LATTICES USING PHONONICS

By

BRYAN D. LLUMIQUINGA

A thesis submitted to the

School of Graduate Studies

Rutgers, The State University of New Jersey

In partial fulfillment of the requirements

For the degree of

Master of Science

Graduate Program in Mechanical and Aerospace Engineering

Written under the direction of

Dr. Jonathan P. Singer

And approved by

____

____

____

New Brunswick, New Jersey

October, 2020

ABSTRACT OF THESIS

SHOCK ATTENUATION IN LATTICES USING PHONONICS

By BRYAN D. LLUMIQUINGA

Thesis Director:

Dr. Jonathan P. Singer

Supersonic aircraft deal with turbulent conditions during flight. These turbulent conditions lead to unwanted stresses that often adversely affects the payload. Several lattices were designed to help attenuate any vibrations or shock that may be experienced by the payload through the concept of phononic crystals. Phononic crystals are periodic composite materials designed to control the propagation of mechanical waves using acoustic band gaps. Three different lattice deigns implemented to a cylindrical shell body were initially explored for this study. Combination lattices consisting of two different lattices within the same geometry were also explored. Combination lattices outperformed their single lattice design counterparts, in terms of frequency suppression, due to the fill factor of mechanically contrasting geometries. All lattice cases evaluated experienced a dominant peak in the frequency domain, near the ring frequency of the cylinder. Low frequency cantilevers were successful in trapping some of the energy caused by the ring mode of the structure.

ACKNOWLEDGEMENTS

First and foremost, I would like to give a huge thank you to Northrop Grumman Innovation Systems (NGIS) in Chandler, Arizona for sponsoring this project. Thanks to this project, I have had the amazing opportunity to be an intern at NGIS and experience what it is like to be in Arizona for the first time. Within NGIS, I would like to thank Scott Rowland, Dr. Paul Hoffecker, Kevin Horn, and the R&D team for all their support while I was there. I remain grateful for the guidance and advice that Scott Rowland provided as a manager. I remain thankful for the mentorship, guidance, and the lessons taught by Dr. Paul Hoffecker as a team lead. Lastly, the support and friendship experienced by my assigned mentor Kevin Horn is something I will never forget. I am grateful for my time at NGIS and look back with great fondness.

Secondly, I would like to sincerely thank my advisor, Dr. Jonathan P. Singer, for all that he has done for me. Thanks to Dr. Singer's guidance and leadership, I have grown as a student and as an overall individual. I am tremendously grateful for Dr. Singer's willingness to take me on as a student and providing me the opportunity to work on this project. I appreciate his mentorship, patience, and his willingness to help whenever needed. Furthermore, I would also like to thank Dr. Andrew Norris and Dr. Mina Pelegri for their support and guidance throughout this project. I would also like to express my thanks to Dr. Norris's student, Matt Kelsten, for all his help.

Lastly, I would like to thank my family and friends for all their support. To my mother, father, and sister, thank you so much for providing your unwavering emotional and financial support. I would not have been able to continue my education without their

help. None of this would have been possible without the support from all the people mentioned. From the bottom of my heart, I thank you all.

DEDICATION

To my mother, father, sister, and the family dog Rocky.

TABLE OF CONTENTS

Contents

LIST OF FIGURES

LIST OF TABLES

CHAPTER 1

INTRODUCTION

The acoustic equivalent of the commonly known photonic crystal is the phononic crystal. Both photonic and phononic crystals belong to the distinct class of metamaterials that are engineered to have properties not seen in nature. Such properties may include a negative refraction index, sound focusing, or wave guiding [4]. Though both photonic and phononic crystals share similar characteristics, they differ significantly. Phononic crystals deal with the propagation of mechanical waves unlike its counterpart, photonic crystals, that deals with the propagation of electromagnetic waves. The inherent characteristics of mechanical waves compared to that of electromagnetic waves demonstrates just how significant the difference between phononic and photonic crystals are. The remainder of this thesis will primarily focus on an application using phononic crystals and their unique ability to form band gaps.

Phononic crystals are periodic composite materials designed to control the propagation of mechanical waves using acoustic band gaps. The first experimental evidence of the existence of acoustic band gaps in periodic structures was proven by Francisco Meseguer and his colleagues in 1995 [5]. The experiment took place at the Material Science Institute of Madrid where Meseguer et al. studied the acoustic characteristics of a sculpture built by Eusebio Sempere [5]. The sculpture consisted of a two-dimensional square array of hollow steel cylinders in air. Meseguer et al. demonstrated that the attenuation of the acoustic waves occurred in a select frequency range due to the multiple interferences of sound waves caused by the periodic arrangement of the tubes. Meseguer et al. found that the sound attenuation was not a result of absorption as steel is very stiff, but the periodic arrangement of the steel tubes. The periodic arrangement of the tubes led to either constructive or deconstructive interference that was dependent on the frequency of the sound waves. Meseguer et al. measured the transmission of the sculpture as a function of frequency and direction. Their results showed that sound traversing perpendicular to the axis of cylinder was attenuated at a frequency of 1670 Hz [5]. Thus, the periodic structure built by Eusebio Sempere exhibited frequency gaps or phononic band gaps where wave propagation was prohibited.

Many studies have used the concept of phononics to manipulate the propagation of mechanical waves. For example, phononic crystals have been used in the development of microfluidic systems particularly with surface acoustic devices. Previous work by Wilson et al., demonstrated that their phononic crystal lattice design could be engineered on non-piezoelectric materials to filter, reflect, or scatter acoustic waves [7]. As a result, Wilson et al. were able to control the microcentrifugation of particles in a manner that is completely dependent on frequency. Previous work by Bourquin et al. demonstrated that by using a phononic crystal, fluid droplets could be shaped by controlling the interaction between the droplets and the acoustic waves by tuning the frequency of excitation [6]. Bourquin et al. developed a cone-shaped phononic crystal with circular cavities that enabled the focusing of energy at chosen locations whose positions were determined by the excitation frequency and the intensity of the phononic crystal [6]. With that, Bourquin et al. were able to shape the field created by the acoustic waves and establish a control over the direction and the amplitude of the interfacial jetting of a sessile drop of liquid on non-piezoelectric materials [6].

This dissertation focuses on the application of phononic crystals for a shock attenuation study in cylindrical lattices. Supersonic launch vehicles go through extreme flying conditions where they are subjected to unwanted stresses that arise from the shock waves and vibrations associated with the turbulence. Through the concept of phononic crystals, several lattices were designed to help attenuate any vibrations or shock that may be experienced by the payload of the launch vehicle. The main objective was dampening waves traveling through a cylinder using single and mechanically contrasting lattices. Suppressing the cylindrical mode using in-plane metamaterials was explored.

CHAPTER 2

PHONONIC CRYSTALS

2.1: Introductory Remarks

Phononic crystals are periodic structure made of at least two different elastic materials with different mechanical properties [1]. Phononic crystals are typically designed to control the propagation of mechanical waves through a structure. When a wave propagates through a periodic structure, phononic crystals use the inherent properties of the wave to create frequency or wavelength ranges where the wave is prohibited from propagating [1]. Frequency or wavelength ranges where a mechanical wave is not allowed to propagate is referred to as a band gap [2]. Before going further into phononic crystals, it is useful to give background information on the behavior of mechanical waves propagating through a material that is considered homogenous.

2.2: Wave Types

Mechanical waves can be classified as two different types of waves based on their different mechanisms for propagation [1]. Mechanical waves propagating within solid structures are considered elastic waves. Mechanical waves propagating within a fluid such as in liquids or gases are acoustic waves. Elastic waves propagating within solid structures will be the primary focus moving forward. Evaluating elastic waves within homogenous materials is important because homogenous materials contain uniform composition and uniform properties throughout which is useful when assessing complex structures. Most of homogeneous materials are made up of periodic arrangements of atoms in space. Thus, evaluating how these atoms interact when subjected to an elastic wave is important. Elastic waves can be further classified based on the behavior of the displacement of the atoms from their equilibrium position when subjected to an elastic wave propagating with wave vector $\vec{k}$.

For a one-dimensional case, an elastic wave can either be transverse or longitudinal based on the direction of its oscillation. When the displaced atoms move perpendicular to the direction of the propagation, the displacement vector of the atoms also moves perpendicular to the direction of the wave and is considered transverse [1]. Conversely, when the displaced atoms move in a direction that is parallel with the direction of the propagating wave, the displacement vector of the atoms also moves along the direction of the wave and is considered longitudinal [1]. For a one-dimensional case, an elastic wave is classified as either transverse or longitudinal based on the displacement vector and the direction of the propagating wave [1].

The mathematical formulas that describe transverse and longitudinal waves, respectively, are

$$\vec{u}_T = Re(\vec{u}_{T0}e^{i(\vec{k}\cdot\vec{r}-\,\omega t)}) \tag{2.1}$$

$$\vec{u}_L = Re(\vec{u}_{L0}e^{i(\vec{k}\cdot\vec{r}-\,\omega t)}) \tag{2.2}$$

where Re is the "real part of", $\vec{k}$ is the wave vector, ω is the frequency, t is time, $\vec{u}_T$ and $\vec{u}_L$ are the displacement vectors for transverse and longitudinal waves, respectively, $\vec{u}_{T0}$ and $\vec{u}_{L0}$ are the displacement vector amplitude for transverse and longitudinal waves, respectively, and $\vec{r}$ is the displacement vector of the atom. Furthermore, transverse and longitudinal waves are governed by the elastic wave equation. The elastic wave equation for transverse and longitudinal equations reduces to:

$$\nabla^2 \vec{u}_T = \frac{1}{c_T^2} \frac{d}{dt^2} (\vec{u}_{T0}) \tag{2.3}$$

$$\nabla^2 \vec{u}_L = \frac{1}{c_L^2} \frac{d}{dt^2} (\vec{u}_{L0}) \tag{2.4}$$

where c_T and c_L are the transverse and longitudinal wave velocities. From the equations governing the transverse and longitudinal waves (i.e. equations 2.3 and 2.4) and the equations describing the transverse and longitudinal waves (i.e. equations 2.1 and 2.2), the dispersion relation between the frequency and wave vector is established.

$$k = \frac{\omega}{c_T} \tag{2.5}$$

$$k = \frac{\omega}{c_L} \tag{2.6}$$

From the dispersion relations, a relationship between the wave number, frequency, and transverse and longitudinal velocity is established. Furthermore, the transverse and longitudinal velocity is derived from the material properties of the solid structure. The lame parameters of the solid structure are used to determine the transverse and longitudinal velocities

$$\lambda = \frac{E\nu}{(1+\nu)(1-2\nu)} \tag{2.7}$$

$$\mu = \frac{E}{2(1+\nu)} \tag{2.8}$$

where λ and μ are lame parameters, E is the Young's modulus of the solid material, and ν is the Poisson's ratio of the solid material. From the lame parameters, the transverse and longitudinal wave speeds are

$$c_T = \sqrt{\frac{\mu}{\rho}} \tag{2.9}$$

$$c_L = \sqrt{\frac{\lambda+2\mu}{\rho}} \tag{2.10}$$

where ρ is the density of the solid material.

In general, the propagation of a mechanical wave in a solid medium is described by the dispersion relation seen in either equations 2.5 or 2.6 for a homogenous medium. For homogenous solids, the dispersion relation is linear, however, for phononic crystals, the dispersion relation becomes complex [2]. As mentioned earlier, phononic crystals are designed to control the propagation of a wave through band gaps. Band gaps being frequency or wavelength ranges where the wave a prohibited from propagating. To get a better understanding on how phononic band gaps form, the concept of acoustic impedance is explored.

2.3: Acoustic Impedance

An important characteristic relating to the propagation of sound within a solid medium is the acoustic impedance. The acoustic impedance of a solid material is the product of its density and its acoustic velocity

$$Z = \rho V \tag{2.11}$$

where Z is the acoustic impedance, V is the acoustic velocity and ρ is the density of the solid. Acoustic impedance allows for the determination of transmission and reflection at the interface between two materials having different acoustic impedances [3]. Mediums that have different impedances and hence different speeds of sound will produce what is known as an impedance mismatch when a sound wave strikes the boundary between the two materials. As a result of the impedance mismatch, some of the wave transmits through while some of it reflects. The bigger the impedance mismatch, the greater the amount of energy that is reflected at the interface between the two materials. If both the impedances are known, the amount of energy that is reflected is

$$R = \left(\frac{Z_2 - Z_1}{Z_2 + Z_1}\right)^2 \tag{2.12}$$

where R is the reflection coefficient, Z_1 is the acoustic impedance of the first material, and Z_2 is the acoustic impedance of the second material. Since the total incident energy must equal the reflected energy and the transmitted energy, the transmitted coefficient T is calculated by subtracting the reflection coefficient from one.

$$T = 1 - \left(\frac{Z_2 - Z_1}{Z_2 + Z_1}\right)^2 \tag{2.13}$$

Apart from acoustic impedance and impedance mismatch, the concept of interference is also introduced. When sound waves combine as they are propagating this is known as interference. Two propagating waves propagating at the same time can interfere with each other constructively if they are in phase with each other [3]. Conversely, two identical waves can interfere with each other destructively if they are out of phase with each other. Destructive interference leads to the complete cancellation of the combining waves. Meanwhile, constructive interference leads to an increase in the amplitude of the combining waves.

Through interference, when a wave propagates through a periodic structure, the formation of a band gap is established and prevents the wave from propagating at certain frequency ranges [2]. To first understand the formation of band gaps is to imagine waves propagating through a one-dimensional phononic crystal made up of alternating layers of two different materials [2]. At the interface between the materials, propagating waves transfer their energy partially to the reflected waves where the interference takes place. If the interference is constructive then the energy of the primary wave is reflected and is prohibited from propagating within the second material. However, if the interference is destructive, then the energy from the incoming wave is transmitted through to the subsequent material and the propagation continues. Hence, constructive interference leads to the formation of band gaps within 1D phononic crystals.

The formation of band gaps through constructive interference is based on the path difference between the interfering waves. Path difference, in this regard, is the difference in path traversed by the interfering waves measured in terms of wavelength. For constructive interference to occur, the path difference between the interfering waves must equal an integer multiple of their wavelength [2]. Hence, since wavelength is inversely proportional to frequency, constructive interference occurs when the lattice parameter, a, of the phononic crystal is comparable to the wavelength [2]. Thus, by manipulating the size of the unit cell of the chosen phononic crystal, the band gap can be tuned to a distinct frequency range.

2.4: Closing Remarks

The frequency range of the band gap depends highly on the structural parameters of the chosen crystal. Furthermore, for a one-dimensional case, the width of the band gap is dependent on the number of alternating layers used [1]. For a one-dimensional case, the band gap can be widened with increasing number of alternating layers [1]. In general, the ratio of the mechanical properties (i.e. density) of the differing materials affects the overall size of the band gap [1]. The larger the ratio, the larger the resultant band gap will be.

Thus far, only a one-dimensional case has been discussed. However, these statements also hold true for two and three-dimensional phononic crystals. For instance, in the three-dimensional case, the size and characteristic of the band gap depends on not only the geometry of the periodic structure, but the relative volume fraction of the materials that form the periodic structure [1]. The ratio of mechanical properties between the materials also affects the size of the band gap for two and three-dimensional crystals. With increasing dimensions, the process of engineering band gaps becomes more complex. As mentioned earlier, a mechanical wave propagates within a solid having different speeds (i.e. longitudinal and transverse speeds). Hence, manipulating a periodic structure such that it has a band gap in different directions becomes quite the challenge.

CHAPTER 3

EXPERIMENTAL SETUP

3.1: Introductory Remarks

Supersonic aircraft go through turbulent flying conditions where they are subjected to extreme stresses that arise from the shock waves and vibrations associated with the turbulence. Often these aircrafts carry sensitive electronics attached to them while navigating through such turbulence at high speeds. Ideally, these electronics would be removed from the launch vehicle and completely mechanically isolated from all vibrations and shock waves. However, to completely isolate these electronics, massive amounts of mass must be added to the launch vehicle which makes this method completely impractical. By adding more mass to the launch vehicle, not only does the vehicle itself become heavier, but the rate of fuel consumption also increases. This scenario is not ideal. This thesis focuses on the application of phononics to attenuate acoustic produced vibrations that may reach the payload. Through the concept of phononic crystals, several lattices were designed to help attenuate any vibrations or shock that may be experienced by the payload.

3.2: Approach

3.2.1: Unit Cell Simulation

When working with unit cells, it is not necessary to draw out every single unit cell out to infinity and not every wave number needs to be considered. Instead, imagine that we fold the infinite diagram such that you are only looking at one characteristic length of the structure. Essentially, instead of plotting the bands as the speed of sound as a function of the wave number, going off to infinity, we fold it back on itself. If there is periodicity in the structure as we see in figure 1, for one of the lattices, we can essentially look at the point where the wave number corresponds to half of a standing wave inside the material.

Inside an infinite material, you can have distinct modes that are phase shifted from one another by half a wavelength. If this is represented inside a real material (i.e. the lattice), two waves that have the same wavelength but are in different materials are going to have different characteristic energies. This means that if it takes more energy to displace material 1 than it does to displace material 2, the same wavelength will now have a higher frequency (i.e. higher energy). Two distinct waves that have the same wavelength, but distinct energies will cause a bandgap to occur.

Bandgaps are necessary for energy dissipation and mitigation. At a band gap, a wave cannot travel through the material thus this represents a band of frequencies where wave propagation is prohibited. Hence, a perfect reflector is created if you have enough of periodic repeat units. To begin setting up the phononic band gap analysis for the kagome lattice (i.e. figure 1), figure 1 had to reduce to its irreducible unit cell form as seen in figure 2. Using COMSOL Multiphysics, the phononic band gap analysis was setup and the geometry of the lattice was created. The unit cell analysis performed in COMSOL Multiphysics utilized the structural mechanicals module. Within the structural mechanics module, the type of physics implemented to the unit cell model was solid mechanics.

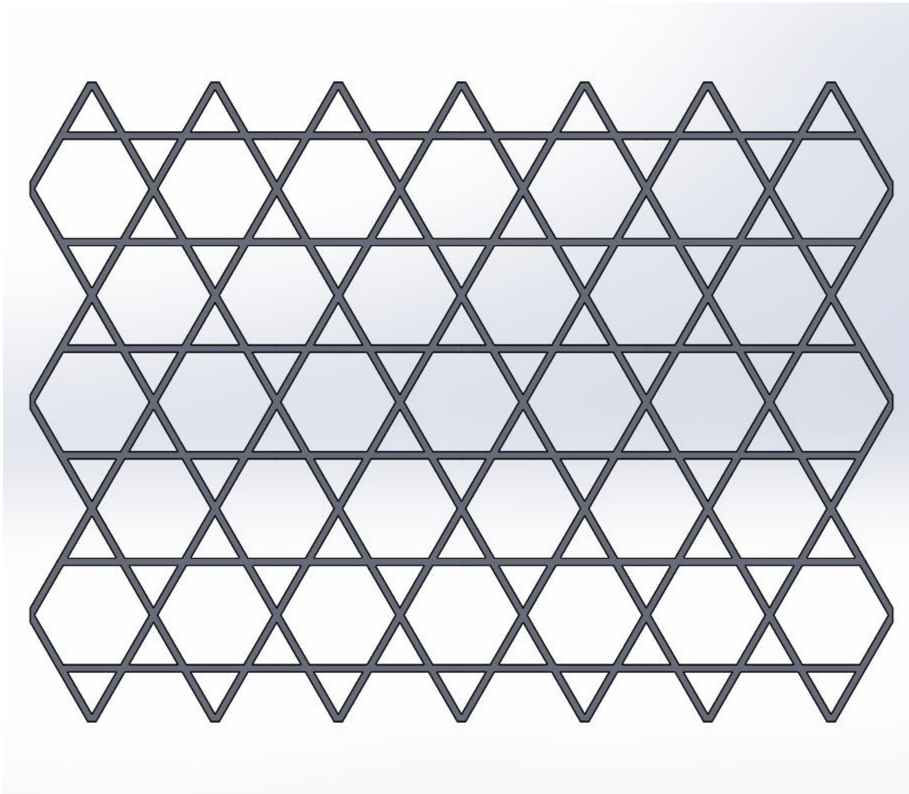

Figure 1: The first lattice referred to as the Kagome lattice. This was first lattice that was analyzed for the shock attenuation study.

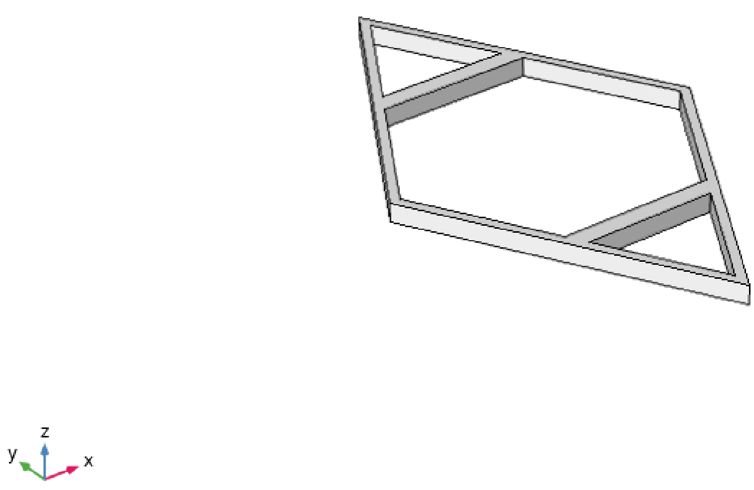

Figure 2: The irreducible unit cell of the kagome lattice as seen in **figure 1.**

Evaluating the frequency response of the kagome lattice required an analysis of the kagome unit cell as an infinite waveguide with Bloch boundary conditions that spanned a for range of wave vectors (wave numbers). For the first approach, since a flat kagome unit cell was evaluated, the Bloch boundary conditions were applied on the faces that were parallel to each other. The Bloch boundary condition is defined as shown in equation 3.1 where the boundary conditions are applied on the parallel faces of the unit cell and the wave number is user selected [8].

$$\vec{u}_{dst} = \vec{u}_{src} e^{-i\vec{k}(\vec{r}_{dst} - \vec{r}_{src})} \tag{3.1}$$

In equation 3.1, $\vec{u}_{src}$ is the displacement field at designated variable for a source, $\vec{u}_{dst}$ is the displacement field at designated variable for a destination, $\vec{k}_F$ is the wave number, $\vec{r}_{src}$ is the spatial coordinate of the boundary where the destination is applied, and $\vec{r}_{dst}$ is the spatial coordinate of the boundary where the destination is applied [8]. Essentially, the Bloch boundary condition constrains the boundary displacements and allows for it to simulate as if there were infinite unit cells. The wavenumber was parametrically swept in an eigenfrequency analysis. From the resultant eigenfrequencies, the dispersion curves for the periodic unit cell was evaluated as a function of the wavenumber. Through this method, a periodic dispersion curve with respect to the wavenumber is plotted where a pattern of curves repeats every $\frac{2\pi}{a}$. The term a here is the distance between the parallel faces or the lattice constant. To get a better understanding of this concept, the concept of the reciprocal-lattice space and the Brillouin zone is briefly discussed.

3.2.2: Reciprocal Lattice Space and Brillouin Zone

Any periodic structure (i.e. the kagome lattice) has an associated point lattice which determines the position of the repeating units [1]. Thus, the point lattice implies that there exists a periodic array of imaginary lattice points associated with the periodicity of the structure. These lattice points have identical surroundings in all directions. These lattice points can be assumed to be at the center of cells that repeat in all directions. By selecting a single cell, arbitrarily, a unit cell can be selected that represents the periodic arrangement that forms the point lattice.

The selected unit cell that makes up the point lattice is characterized by the primitive lattice vectors $\vec{a}_n$, where n is dependent on the dimension size. This all holds valid for two- and three-dimensional cases. The primitive lattice vectors that define the unit cell construct the entire point lattice through translation [1]. For example, for the two-dimensional case, the corresponding lattice point $\vec{R}$ in space that repeats and makes up the point lattice is defined as an array of regularly spaced lattice points [1].

$$\vec{R} = n_1\vec{a}_1 + n_2\vec{a}_2 \tag{3.2}$$

Similarly, for a three-dimensional case:

$$\vec{R} = n_1\vec{a}_1 + n_2\vec{a}_2 + n_3\vec{a}_3 \tag{3.3}$$

Where n_1, n_2, and n_3 are arbitrary integer numbers that correspond to the lattice point $\vec{R}$ in space.

For a case where a plane wave propagating through a lattice with a wave vector $\vec{k}$ does not match the same periodicity of the lattice, an associated reciprocal lattice is introduced. By not having the same periodicity it is meant that, $e^{i\vec{k}\cdot\vec{r}} \neq e^{\overline{\iota k}\cdot(\vec{r}+\vec{R})}$, where $\vec{R}$ is the corresponding lattice point vector in space that makes up the point lattice. To establish a reciprocal lattice, specific wave vectors must allow for the plane wave to satisfy the periodicity of the lattice. These specific wave vectors denoted by $\vec{G}$ satisfy the periodicity of the lattice if $e^{i\vec{G}\cdot\vec{r}} = e^{\overline{\iota G}\cdot(\vec{r}+\vec{R})}$. Furthermore, these wave vectors $\vec{G}$ are referred to as set of reciprocal lattice vectors and they make up the reciprocal lattice. Like the point lattice and its primitive lattice vectors, the reciprocal lattice can be defined using its reciprocal lattice primitive vectors as shown.

For a two-dimensional case:

$$\vec{G} = m_1\vec{b}_1 + m_2\vec{b}_2 \tag{3.4}$$

Similarly, for the three-dimensional case:

$$\vec{G} = m_1\vec{b}_1 + m_2\vec{b}_2 + m_3\vec{b}_3 \tag{3.5}$$

Where m_1, m_2, and m_3 are arbitrary integer numbers, $\vec{b}_1$, $\vec{b}_2$, and $\vec{b}_3$ are reciprocal lattice primitive vectors.

For a two-dimensional case, the reciprocal lattice primitive vectors are defined based on the primitive lattice vectors that define its point lattice as shown:

$$\vec{b}_1 = \frac{2\pi(\vec{a}_2\times\vec{z})}{\vec{a}_1\cdot(\vec{a}_2\times\vec{z})} \tag{3.6}$$

$$\vec{b}_2 = \frac{2\pi(\vec{z}\times\vec{a}_1)}{\vec{a}_1\cdot(\vec{a}_2\times\vec{z})} \tag{3.7}$$

For a three-dimensional case, the reciprocal lattice primitive vectors are defined based on the primitive lattice vectors that define its point lattice as shown:

$$\vec{b}_1 = \frac{2\pi(\vec{a}_2 \times \vec{a}_3)}{\vec{a}_1 \cdot (\vec{a}_2 \times \vec{a}_3)} \tag{3.8}$$

$$\vec{b}_2 = \frac{2\pi(\vec{a}_3 \times \vec{a}_1)}{\vec{a}_1 \cdot (\vec{a}_2 \times \vec{a}_3)} \tag{3.9}$$

$$\vec{b}_3 = \frac{2\pi(\vec{a}_1 \times \vec{a}_2)}{\vec{a}_1 \cdot (\vec{a}_2 \times \vec{a}_3)} \tag{3.10}$$

Since the kagome lattice unit cell corresponds to a triangular two-dimensional point lattice and thus a triangular two-dimensional reciprocal lattice, using equations 3.6 and 3.7 the reciprocal lattice primitive vectors are defined as shown:

$$\vec{b}_1 = \frac{2\pi}{a}\hat{\imath} - \frac{2\pi}{a\sqrt{3}}\hat{\jmath} \tag{3.11}$$

$$\vec{b}_2 = \frac{4\pi}{a\sqrt{3}}\hat{\jmath} \tag{3.12}$$

Where *a* is the lattice constant which refers to the physical dimension of the selected unit cell. The primitive lattice vectors for a two-dimensional triangular lattice is defined as shown.

$$\vec{a}_1 = a\hat{\imath} \tag{3.13}$$

$$\vec{a}_2 = \frac{a}{2}\hat{\imath} + \frac{a\sqrt{3}}{2}\hat{\jmath} \tag{3.14}$$

An illustration of the point lattice and the reciprocal lattice for a two-dimensional triangular lattice is shown in figure 3.

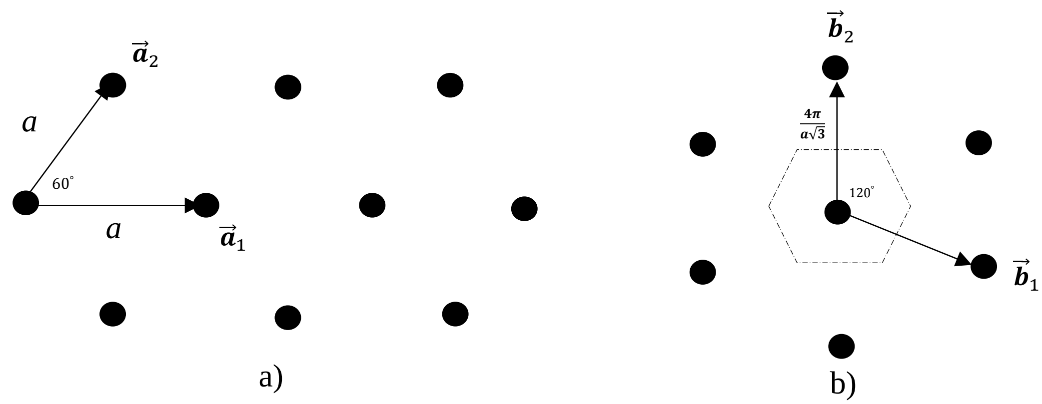

Figure 3: a) Triangular point lattice with its associated primitive vectors and unit cell. b) The associated reciprocal lattice of the point lattice with its associated reciprocal lattice primitive vectors and unit cell.

An important feature when modelling an infinite phononic crystal (i.e. the kagome unit cell) to take into consideration is the fact that the dispersion relation $\omega = \omega(\vec{k})$ is periodic. Thus, only a select few of wave vectors $\vec{k}$ need to be calculated. Taking into consideration the reciprocal lattice, the dispersion relation also must satisfy the following equation where $\vec{G}$ is the reciprocal lattice vector that makes up the reciprocal lattice.

$$\omega(\vec{k}) = \omega(\vec{k} + \vec{G}) \tag{3.15}$$

This periodicity shown in equation 3.15 demonstrates that a frequency ω with a corresponding wave vector $\vec{k}$ will have the same frequency ω value with a corresponding wave vector of $\vec{k} + \vec{G}$. Thus, this periodicity allows for only a specific subset of wave vectors to be calculated to establish and plot a corresponding dispersion relation. These specific wave vectors that determines the dispersion relation makes up the Brillouin Zone. Evaluating wave vectors outside the Brillouin zone is considered unnecessary since the dispersion relation is periodic. The Brillouin zone that correspond to the triangular lattice is shown in figure 3b. The area enclosed within the hexagon is the Brillouin zone and its limits are determined by a locus of points that are equidistant to surrounding points in the reciprocal lattice [1].

Implementing the concept of the reciprocal lattice and the Brillouin zone into the kagome unit cell model involved applying the appropriate boundary conditions to the unit cell. Within the solid mechanics branch in COMSOL Multiphysics exists the periodic condition. This periodic condition allows for the ability to prescribe the displacements on two different sets of boundaries with the identical geometries as related, as seen in periodic structures. Within this periodic boundary condition exists a couple of different types of periodicity that can be prescribed. The Floquet (Bloch) periodicity was selected for its ability to be used in frequency domain problems with a spatial periodicity of the geometry and solution.

As mentioned earlier, in section 3.2.1, the Floquet (Bloch) allows for the selected unit cell to be modelled as an infinite wave guide by selecting the appropriate boundaries. As shown, in figure 4, the boundaries selected for the kagome unit cell were parallel from each other and COMSOL Multiphysics designated these boundaries as a source and a destination, respectively. When applying the Floquet (Bloch) condition in COMSOL Multiphysics, the user must apply a $\vec{k}$ vector for Floquet (Bloch) periodicity. This $\vec{k}$ vector refers to the $\vec{k}$ vector described in equation 3.1 and it is known as the wave number for the excitation. Since the kagome unit cell corresponds to a triangular lattice (i.e. figure 3), the corresponding components for the $\vec{k}$ vector inputted for the Floquet (Bloch) periodicity were the reciprocal lattice primitive vectors (i.e. equations 3.11 and 3.12). An eigenfrequency analysis was performed where the wave number would be parametrically swept while solving for eigenfrequencies.

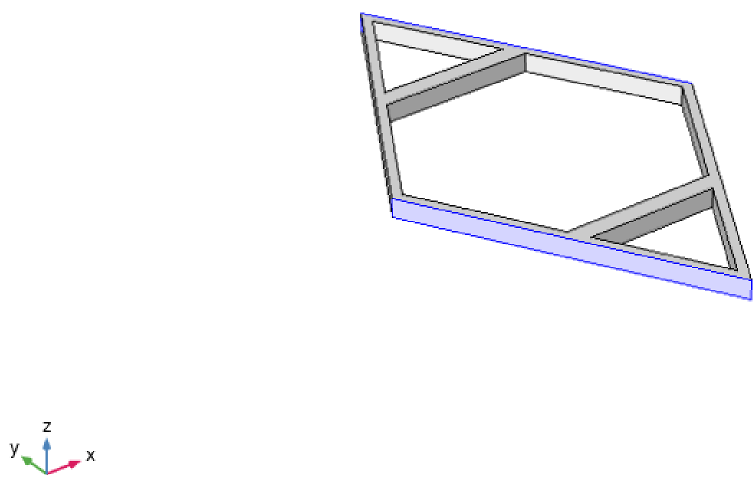

Figure 4: The application of the Floquet (Bloch) boundary condition to one of the parallel sides (highlighted).

3.2.3: Cylindrical Strip Simulations

Another approach used to analyze lattices for this shock attenuation study was using thin cylindrical shells. Different lattices were designed and made in COMSOL Multiphysics and were implemented into a cylindrical shell geometry. The thickness of the shell was made such that the thickness of the shell was much smaller than the overall height of the cylinder (H>>t) where H is the height of the cylinder and t is the shell thickness. For confidentiality reasons, the dimensions of the lattices and the cylinder will not be disclosed in this thesis. Furthermore, by applying the lattices to a cylindrical shell geometry, this introduced a curvature into the lattice unit cells. Analyzing how different lattices perform when subjected to a pulse within a cylindrical shell in a time dependent study was the primary focus of this portion of the study.

To begin setting up this simulation, the cylinder had to be designed in a way to appropriately account for any possible reflections from the propagating wave once it reached the end of the cylinder. Ideally, a perfectly matched layer (PML) would be the ideal choice for this scenario since PMLs are perfect absorbers to any propagating wave. However, since PMLs in COMSOL Multiphysics tend to work only in frequency domain, it could not be implemented to this time domain problem. For this transient problem, infinite element domains were implemented on opposite sides of the cylinder as shown in figure 5. Several partitions were also implemented onto cylinder to allowed for designated areas for the infinite element domains, lattice, and to establish a pulse.

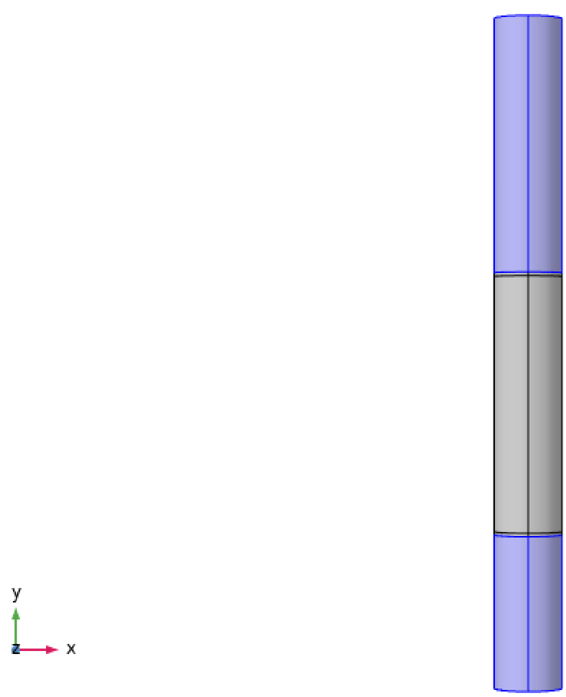

Figure 5: The initial cylinder made in COMSOL Multiphysics with applied infinite domains highlighted blue.

The infinite element domains were selected because instead of having the wave be absorbed as in the case of a PML, an infinite domain would do exactly what its name implies. The infinite domain would allow for the selected domain to behave as if it were infinite. It is a scaling feature that allows for any incoming wave to essentially propagate through an infinite domain. Through this implementation, reflections were minimized. The default stretching function of the infinite domain is defined as shown [9].

$$f(\xi) = \frac{\xi}{\gamma - \xi}\Delta_p \tag{3.16}$$

Where ξ is a dimensionless parameter that varies from 0 to 1 over the selected infinite domain, Δ_p is defined pole distance, and γ is the defined parameter COMSOL Multiphysics defines that must be greater than one as shown.

$$\gamma = \frac{\Delta_p + \Delta_s}{\Delta_s} > 1 \tag{3.17}$$

The scaled thickness Δ_s of the infinite domain and the pole distance Δ_p are both user defined values. The scaled thickness Δ_s, however was kept to its default value of 1e3*dGeomChar, where dGeomChar is the characteristic geometry dimension given by COMSOL Multiphysics. Keeping the scaled thickness Δ_s at its default value allows for the domain to be scaled to a very large value, but not quite to infinity. The reason for this is because scaling to infinity would result in numerical issues within the model. The pole distance relates to the default stretching function described in equation 3.16. In equation 3.16, a singularity occurs when ξ = γ, however since γ is greater than 1, this occurs outside the infinite domain. The pole distance Δ_p controls how far this singularity occurs. The pole distance Δ_p was kept at its default value of dGeomChar to ensure that it is small enough compared to the scaled width Δ_s. By ensuring that Δ_p is much smaller than Δ_s, the coordinate stretching becomes nonlinear and exhibits a 1/r type behavior, where r is the distance form any sources or inhomogeneities [9]. This type of behavior is optimal for mesh resolution.

With the implementation of the infinite domains, establishing a pulse on the cylinder was the next step. The pulse was sourced at one of the partitions made near the end of the cylinder, right above the bottom infinite domain. A boundary probe was implemented on another partition located on the other end of the cylinder, below the top infinite domain to act as a detector to any propagating wave. This detector was used to gather data that included the out of plane displacement. Figure 6 illustrates where the source pulse and the detector were placed. The locations of the source and the detector had some spacing between the infinite domain to avoid any issues with the infinite domains.

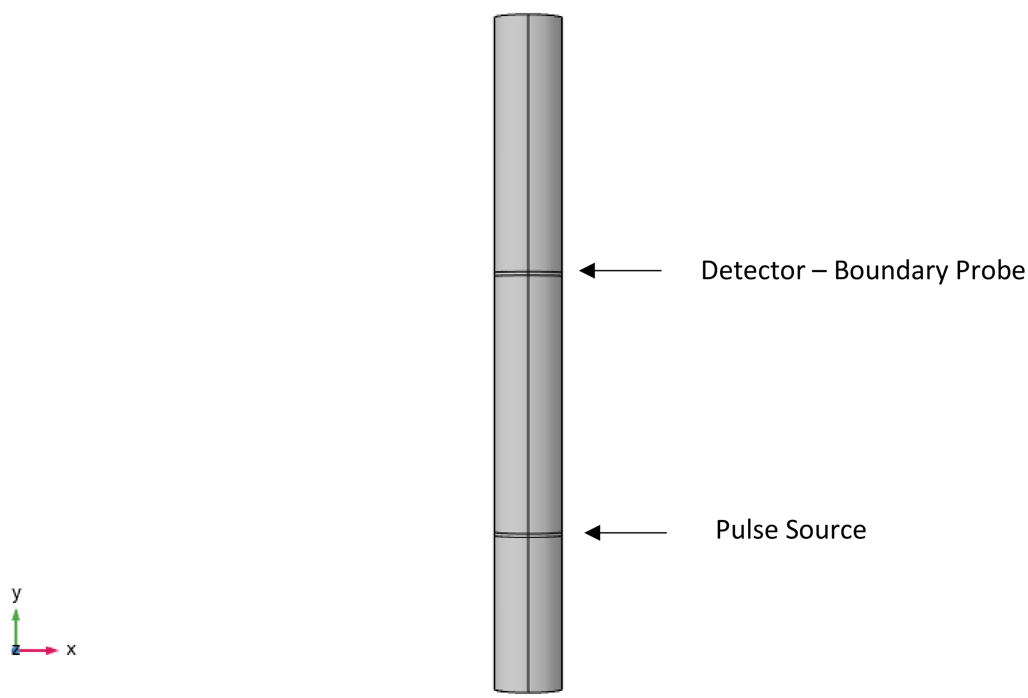

Figure 6: Source and detector location on the plain cylinder.

The pulse used for this model was very sharp and was implemented at the source. The half sinusoidal pulse had a frequency of 5000 Hz and had a period of 1e-4 seconds as shown in figure 7. To implement this pulse, an edge load was used and implemented at the inner edges of the cylinder that were made from a partition. Applying an edge load in COMSOL Multiphysics required a force expression. Since the axis of the cylinder was in the y-direction as shown in figure 6, to get a radial pulse going, the force components of interest were only in the x and z-directions. Equations 3.18 and 3.19 show the force expressions implemented into the edge load that acquired a radial pulse.

$$F_x = (F_f)(anl(t))\frac{x}{\sqrt{x^2+z^2}} = F_f\,\frac{x}{R} \tag{3.18}$$

$$F_z = (F_f)(anl(t))\frac{z}{\sqrt{x^2+z^2}} = F_f\,\frac{z}{R} \tag{3.19}$$

Where x represents the x-coordinates of the model, z represents the z-coordinates of the model, R represents the radial coordinates of the model in cylindrical coordinates, anl(t) is the analytical expression for the half sinusoidal pulse within COMSOL Multiphysics and F_f is a forcing factor that represents an amplitude used in the forcing expressions. To avoid any non-linearities with the model, a forcing factor F_f of 1e-6 was selected to ensure that an initial pulse would not be too great for the designed cylinder. Lastly, since the axis of the cylinder was in the y-direction, the force expression for the y-direction was kept at zero (i.e. $F_y = 0$).

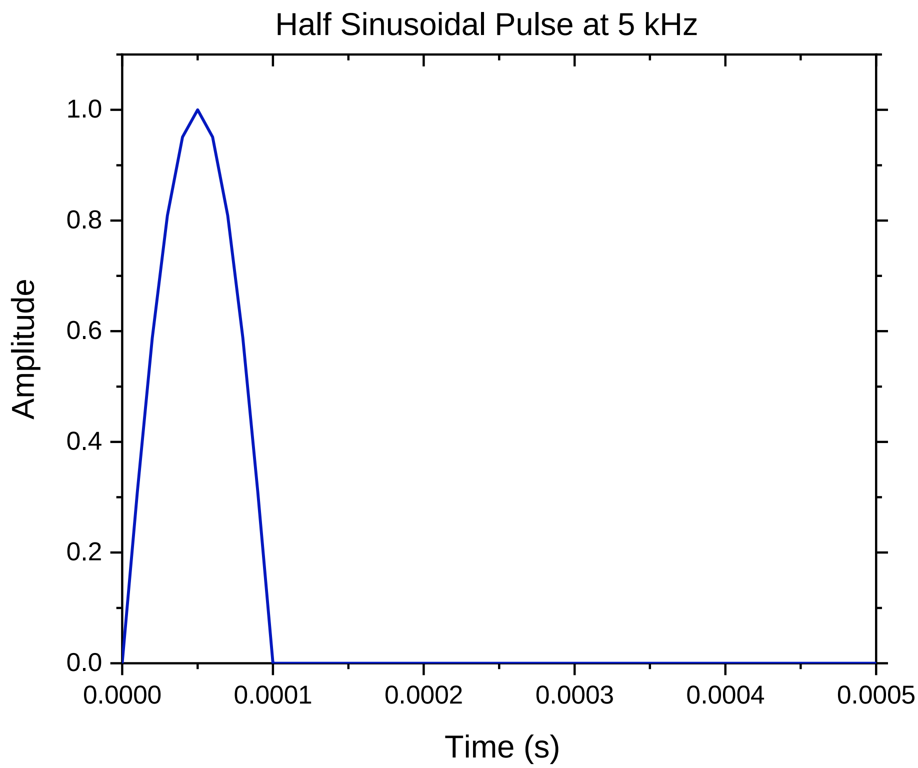

Figure 7: A half sinusoidal pulse used at 5000 Hz with a period of 1e-4 seconds.

The implementation of the lattice onto the shell was the subsequent step in setting up the cylindrical shell. As mentioned earlier, the kagome lattice (i.e. figure 1) was analyzed for this study. The addition of the kagome lattice onto the cylindrical shell was made in COMSOL Multiphysics and is shown in figure 8. The geometry shown in figure 8 was made to be highly parametrized. By doing so, variables such as the radius of the cylinder, the height of the cylinder, the thickness of the shell, the position where the partitions were made could be controlled. Regarding the unit cells, these were made such that the number of unit cells arrayed along the axis of the cylinder could be controlled within a fixed space of the cylinder. Also, the ability to control the number of unit cells revolving around the cylinder was also parametrized.

Since the lattice was fitted within a fixed length of the cylinder, whenever the desired number of arrayed unit cells or the number of unit cells revolving around the cylinder would change, the size of the unit cells would alter appropriately to fit within the fixed space. The example shown in figure 8, shows the kagome unit cell being arrayed in the y-direction 10 times while being revolved around the cylinder 20 times. Hence, there are 20 kagome unit cells that make up a full revolution around the diameter of the cylinder and each of them are being arrayed on top of each other 10 times. Thus, a total of 200 kagome unit cells are in the cylinder shown in figure 8.

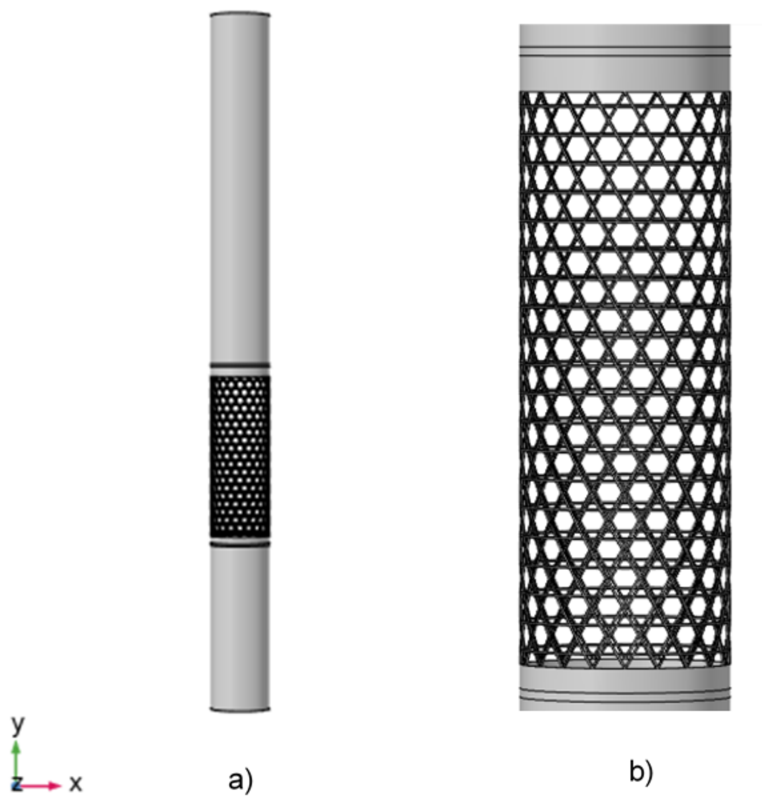

Figure 8: a) A full cylindrical view of the kagome lattice implemented. b) A zoomed in view of the kagome lattice on the cylindrical shell at N = 20.

With the ability to have multiple variables parameterized, it was best to keep certain parameters fixed for potential comparison purposes. For instance, the height, the radius, the size of the infinite domains, and the portion of the cylinder where the lattice was implemented were all kept constant. The structure was modified such that the unit cells for this structure changes accordingly based on the desired number of unit cells revolving around the cylinder at a constant diameter and height. The combination of the arc length equation and the circumference of a circle equation helped accomplish this. The equation used is shown in equation 3.20.

$$S = \frac{2\pi R}{N} \tag{3.20}$$

Where S is the arc length of a unit cell, R is the radius of the cylinder, and N is the number of desired unit cells that are revolved around the cylinder.

Furthermore, two other lattice designs were also added to cylindrical shell models. The second lattice design was referred to as the diamond lattice. Like the kagome lattice, the diamond lattice was similar in that it was also a triangular lattice, but with no horizontal bars in its unit cell structure. A flat diamond lattice unit cell is shown if figure 9. The diamond lattice fully integrated onto a cylindrical shell is shown in figure 10.

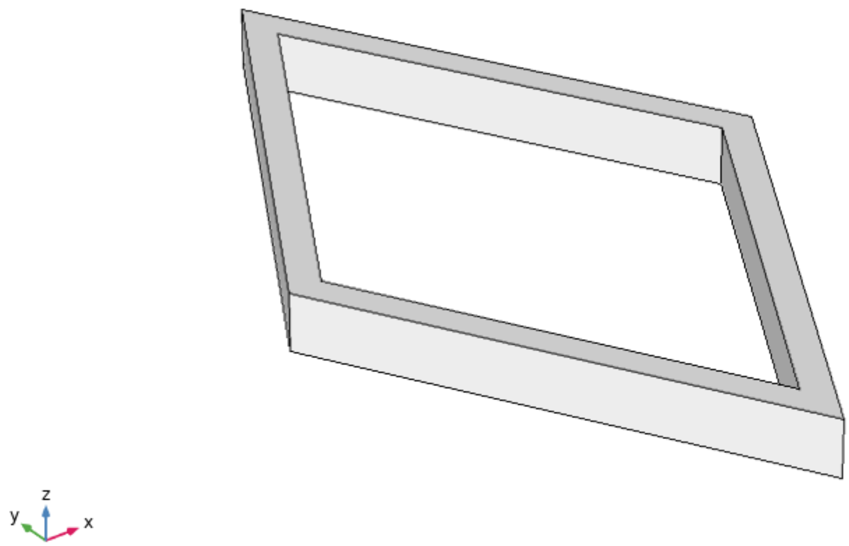

Figure 9: The diamond lattice unit cell.

Figure 10: a) A full cylindrical view of the diamond lattice implemented to a cylindrical shell. b) A zoomed view of the diamond lattice on the cylindrical shell at N = 20.

The third lattice analyzed was considered a hybrid lattice of the kagome and diamond lattice. This hybrid lattice was referred to as a mixed lattice. Unlike, the prior two lattices, the unit cell of the mixed lattice was rectangular. The unit cell of the mixed lattice is shown in figure 11. The mixed lattice fully integrated onto a cylindrical shell is shown in figure 12. The diamond and the mixed cylindrical models were modelled the same way the kagome cylinder model was modelled described earlier.

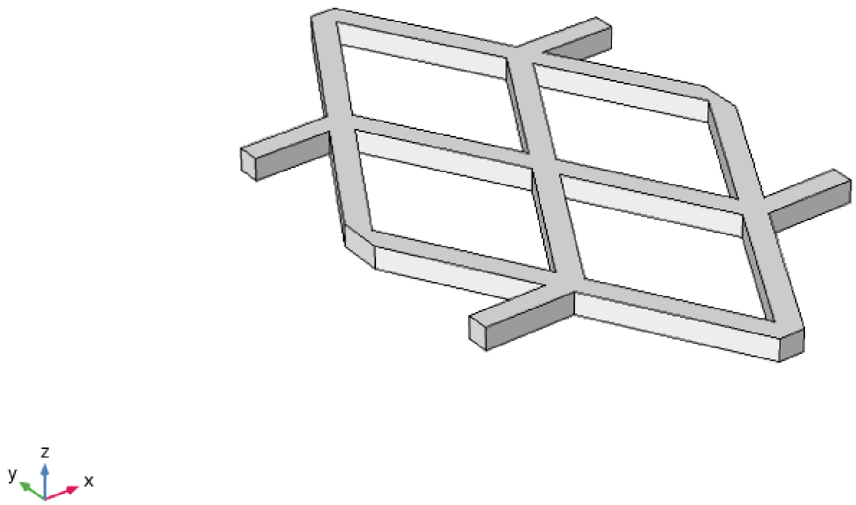

Figure 11: The mixed lattice unit cell.

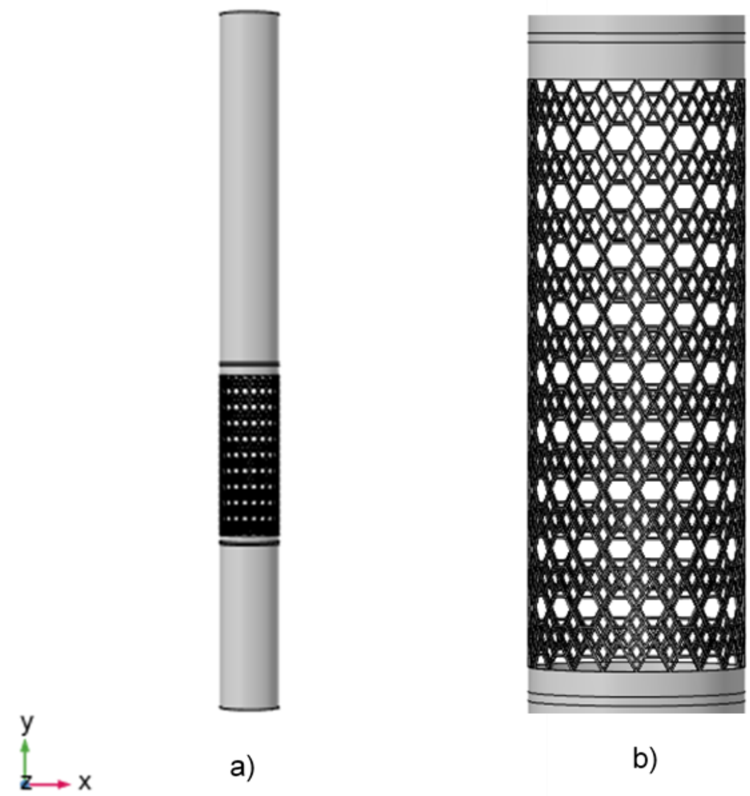

Figure 12: a) A full cylindrical view of the mixed lattice implemented to a cylindrical shell. b) A zoomed view of the diamond lattice on the cylindrical shell at N = 20.

After the implementation of the lattice, it became apparent that the addition of a lattice onto a full cylindrical shell massively increased the degrees of freedom of the system. Thus, making it very computationally expensive. To combat this, the cylinder model was redesigned such that only a portion of the cylinder would be analyzed. By doing so, only a strip of the cylinder for each lattice would be taken into consideration. Since the entire model was made to be highly parametric, reducing the cylinder to a strip form was easily done through work planes and partitions.

The size of the strip depended highly on the N-value selected. As mentioned earlier, the N-value establishes how many unit cells revolve around the cylinder. So, if N were equal to 20, the cylinder was redesigned to cut out a strip that makes up 1/20 of the original cylinder. The unit cells would change in size accordingly with changing N-values to fit. An example of the kagome cylindrical shell model being reduced to its strip form for the case of N equaling 20 is shown in figure 13. The kagome, mixed and diamond cylinder models were all reduced to their strip form as shown in figure 14.

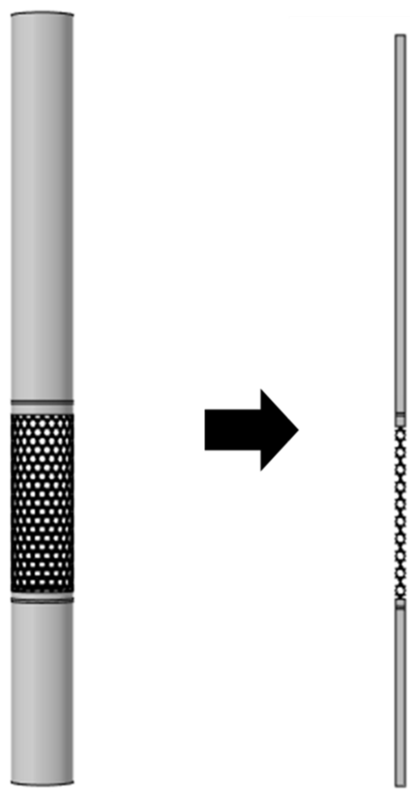

Figure 13: The cylindrical shell with the kagome lattice being reduced to 1/20 of its original shape for a N = 20 case.

Figure 14: The strip form of the a). kagome, b). diamond, and c). mixed lattice for a N = 20 case corresponding to 10-unit cells arrayed together.

To appropriately simulate these strips as if they were still in a full cylindrical body, appropriate boundary conditions had to be applied at the sides of the strips where the cuts were made. Rollers were implemented at the sides of the strip as they can be considered mirror boundary conditions. The roller node in COMSOL Multiphysics adds a roller constraint at the selected boundary that enables zero displacement in the direction normal to the boundary. The boundary, however, is still free to move in the tangential direction. This behavior allows the sides of the strip to act as a mirror. Thus, the strip would be simulated as if it were still a part of the cylinder without having the full cylinder. Figure 15 demonstrates where the roller boundary condition was implemented on the strip.

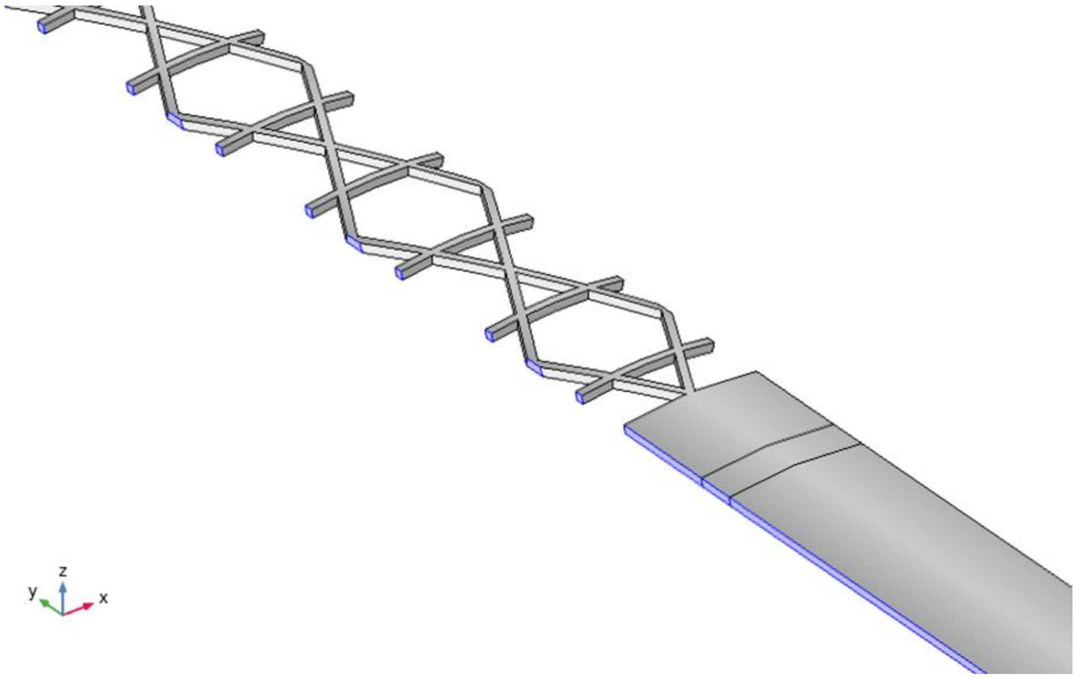

Figure 15: The roller boundary condition being implemented on the kagome strip at one of its sides (highlighted blue).

Further analysis of the lattice strips looked at combination lattices formed by different combinations of the kagome, diamond, and mixed lattices. These lattice strips were referred to as half and half strips since half of the arrayed lattice unit cells consisted of one type of lattice and the other half consisted of another type of lattice. Three half and half lattice strips were analyzed for this portion of the study. One case looked at a lattice strip consisting of the kagome and diamond lattice. Another case looked at a lattice strip consisting of the kagome and mixed lattice. The final case looked a lattice strip consisting of the mixed and diamond lattice. Analysis of which lattice perform the best in terms of frequency reduction in the frequency domain was the objective. The half and half lattice strips analyzed are shown in figure 16.

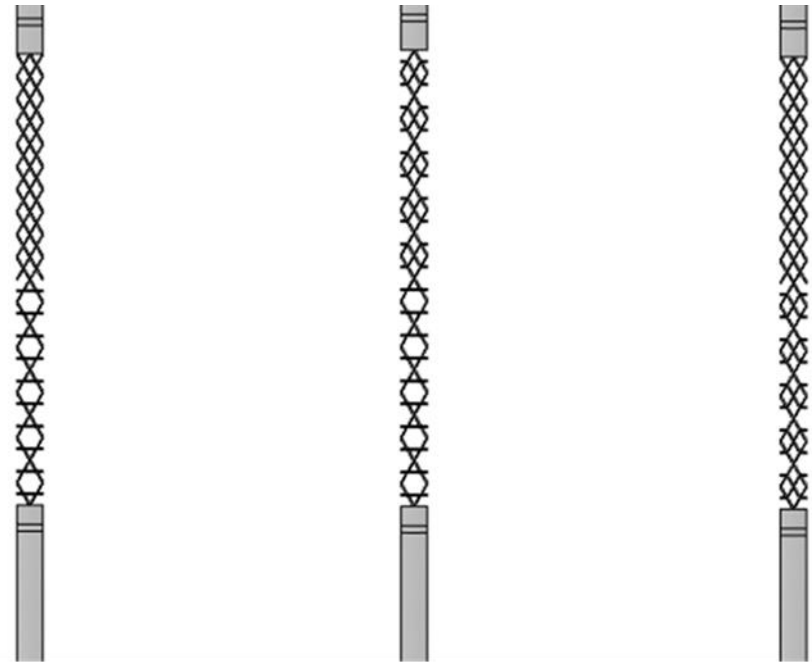

a). b). c).

Figure 16: The half and half combination lattices formed by different combinations of the kagome, diamond, and mixed lattices. a) Kagome/diamond lattice strip, b) Kagome/mixed lattice strip, and c) the Mixed/diamond strip for a N = 20 case.

Further analysis of the lattices also looked at alternating unit cells within the strip. Like the prior analysis that looked at half and half lattice combinations, these lattice strips were constructed in a way such that the unit cells of two different lattices would alternate continuously within the array of the strip. Thus, creating a new periodicity within the structure. Like the half and half analysis, the alternating unit cell strips consisted of the kagome/diamond, kagome/mixed, and mixed/diamond cases. The strips analyzed that consisted of alternating unit cells are shown in figure 17.

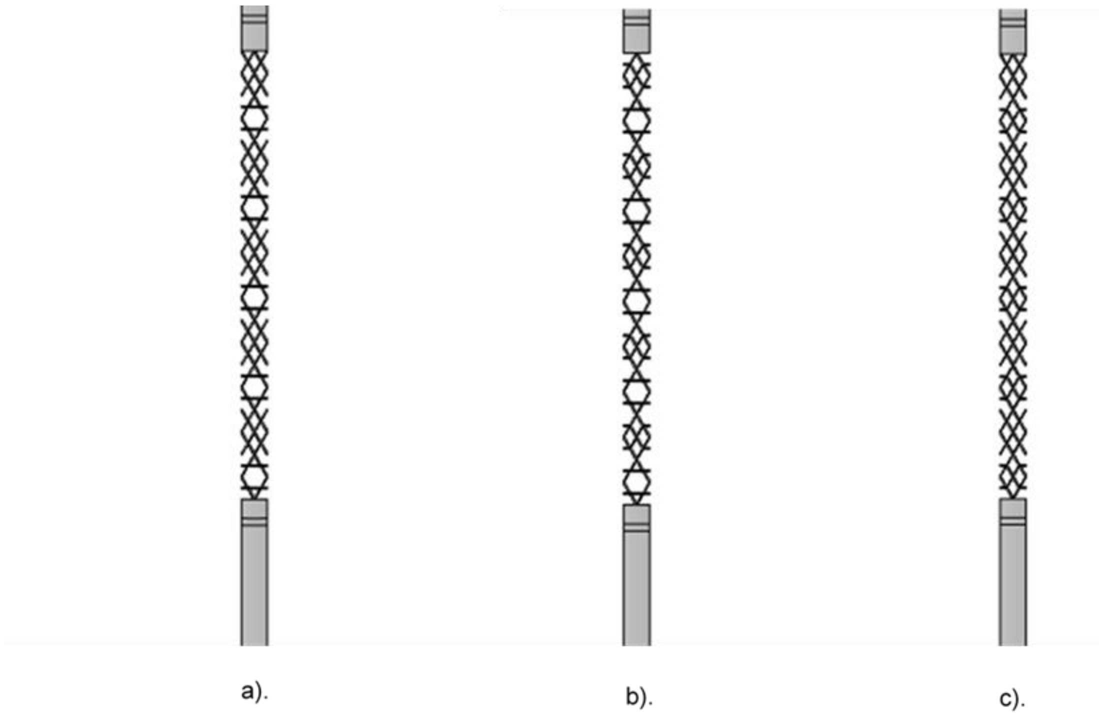

Figure 17: The alternating unit cell lattices formed by different combinations of the kagome, diamond, and mixed lattices. a) Alternating kagome/mixed lattice strip, b) Alternating kagome/diamond lattice strip, and c) Alternating mixed/diamond lattice strip for a N = 20 case.

An analysis of individual lattices, half and half lattices, alternating unit cell lattices was performed to see which lattice variation performed the best in terms of frequency attenuation in the frequency domain. Since time dependent simulations were ran for all these cases, a Fourier transform was implemented to see the results in the frequency domain. As a metric of comparison, a plain strip cut out of a plain cylinder was also analyzed to act as a baseline. The plain strip is shown in figure 18.

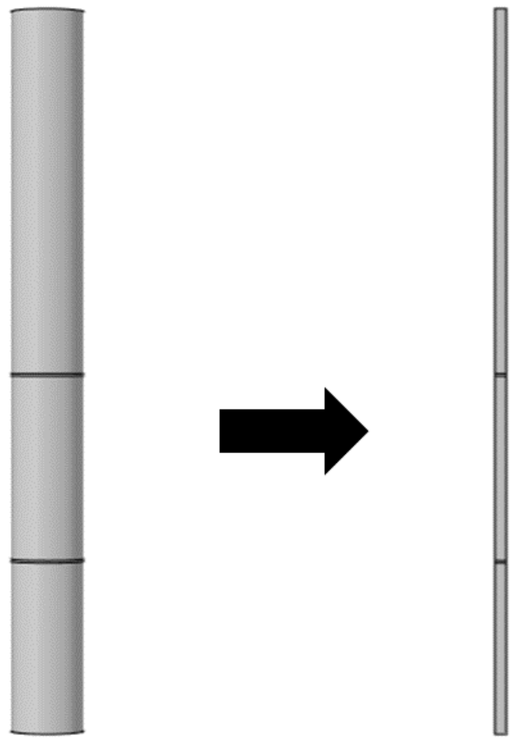

Figure 18: The plain strip analyzed as a baseline for lattice comparison cut from a plain cylindrical shell. The size of this strip is identical to the size of the lattice strip with corresponding N-value. The example shown here is a plain strip for a N = 20 value strip.

Regarding the meshing, COMSOL Multiphysics has a physic-induced meshing sequence that was implemented to all the lattices mentioned. The corresponding physics was to the solid mechanics. The element size was set to extra fine. Regarding the time dependent solver, to get the desired frequency range in the frequency domain up to 5000 Hz, the solver's timestep was set to 1e-4 seconds. The solver ran from 0 to 0.1 seconds. The relative tolerance was set to 1e-7. The tolerance setting controlled the internal timesteps taken from the solver. The initial timestep was set to 1e-6 seconds with a maximum allowed timestep of 1e-5 seconds. The time stepping method taken by the solver was the generalized alpha method.

In collaboration with other research groups within the mechanical engineering department at Rutgers University, the material properties of the models were determined. Experimental data on proprietary sample materials led to the establishment of the elastic modulus, poison’s ratio, and density of the models. In the next chapter, the results of the analysis described in this chapter will described.

CHAPTER 4

RESULTS AND DISCUSSION

4.1: Introductory Remarks

In this chapter, the results from the analysis described in chapter 3 will be discussed. The analysis perform on the flat kagome unit cell will be discussed. Furthermore, the time dependent results from the cylindrical shell strips will also be discussed. An eigenfrequency analysis with Floquet periodicity was performed on the flat kagome unit cell leading to the establishment of the band diagram for the unit cell. All time dependent simulations had identical study conditions. All time dependent simulations ran from 0 to 0.1 seconds with a constant time step of 1e-4 seconds and a maximum time step of 1e-5 seconds. The solver's relative tolerance was set to 1e-7.

A half sinusoidal pulse was setup at the source (figure 7) with a detector set up on the other end of the cylindrical strip. The detector collected the out of plane displacement data from the propagation cause from the pulse. The out of plane displacements from the time dependent simulations were transformed to the frequency domain through a Fourier transform. Characterizing different lattices and establishing which lattice performed had the lowest frequency response in the frequency domain was the objective.

4.2: Unit Cell Analysis

The flat kagome lattice unit cell (figure 4) was evaluated using eigenfrequency analysis. The Floquet boundary conditions were implemented to the unit cell to ensure that the unit cell would be simulated as an infinite periodic waveguide. The wavenumber was parametrically swept from 0 to 0.5 in increments of 0.1. The resultant band diagram is shown in figure 19. The first 20 eigenfrequencies were extracted from this eigenfrequency analysis.

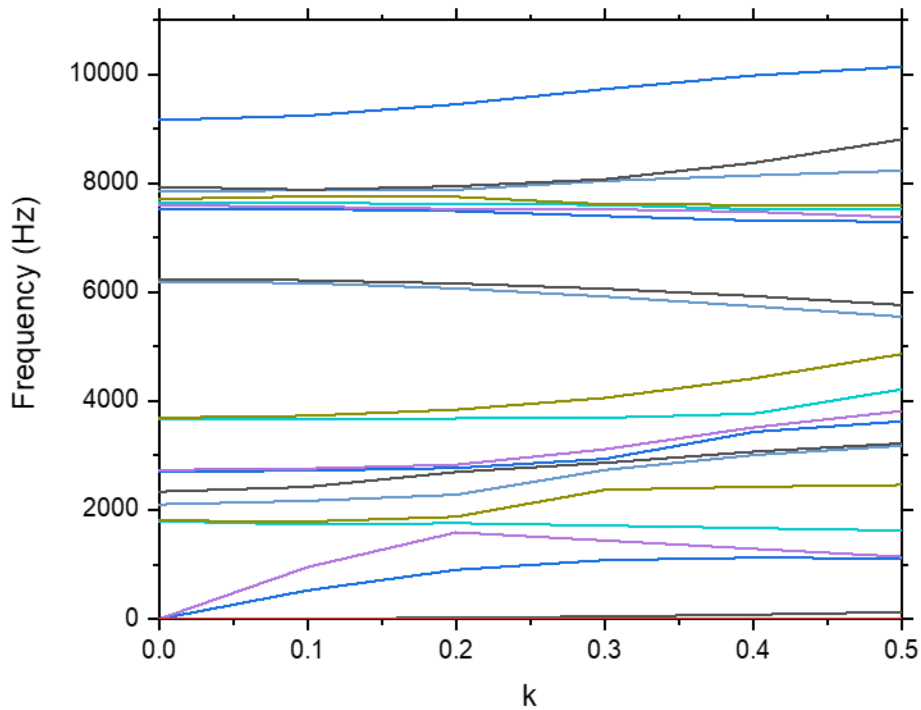

Figure 19: The band diagram of the flat kagome unit cell from a parametric sweep of the wave number k.

When dealing with periodic unit cells, you naturally end up with band gaps as seen at 7000 Hz in figure 19. By band gaps, it is referred to as a frequency region where vibrations are isolated. The band diagram assists in determining where a band gap may exist for the analyzed structure. When a band diagram is generated, it is apparent that many types of deformations exist. Within these propagating modes, also exists standing energy. Standing modes are modes that provide no effect on the direction that the energy is propagating towards. Standing modes provide free energy and are just more deformation within the material. The type of deformation of interest for this project is the bending mode or the out of plane deformation mode.

An initial step for this project was to essentially program the extraction of the out of plane modes and none of that standing energy to characterize the material. Since the modes were periodic, each displacement was mapped to another displacement plus a phase shift due to the propagation which also known as Block periodicity. However, it became apparent that the flat modes of the flat kagome unit cell did not resemble the curve modes of a kagome unit cell within a cylindrical body. The general idea was remained however, in that the curved geometry could be optimized to control where a band gap could occur. Overlapping different band gaps to get the benefits of each in terms of making more band gaps and making the dispersion vary was the goal of the cylindrical models with different lattices implemented.

4.3 Cylindrical Shell Strip Analysis

The kagome lattice strip (figure 14a) was the first strip to be analyzed. The out of plane displacement was collected and outputted by the set detector. The out of plane displacement from the detector was transformed to the frequency domain through a Fourier transform. Since the structure was highly parametric, the first case considered was at N = 20. The time domain response at the detector for the out of plane displacement and its transformation to the frequency domain are shown in figures 20 and 21, respectively.

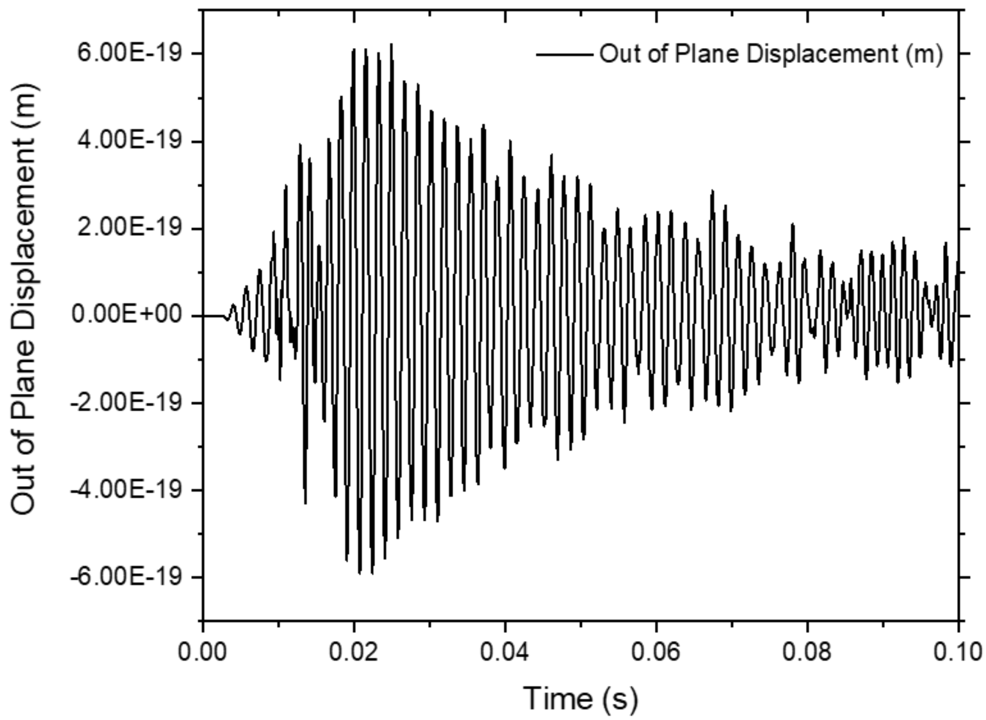

Figure 20: The out of plane displacement of the kagome strip at the detector as a function of time for a N = 20 case.

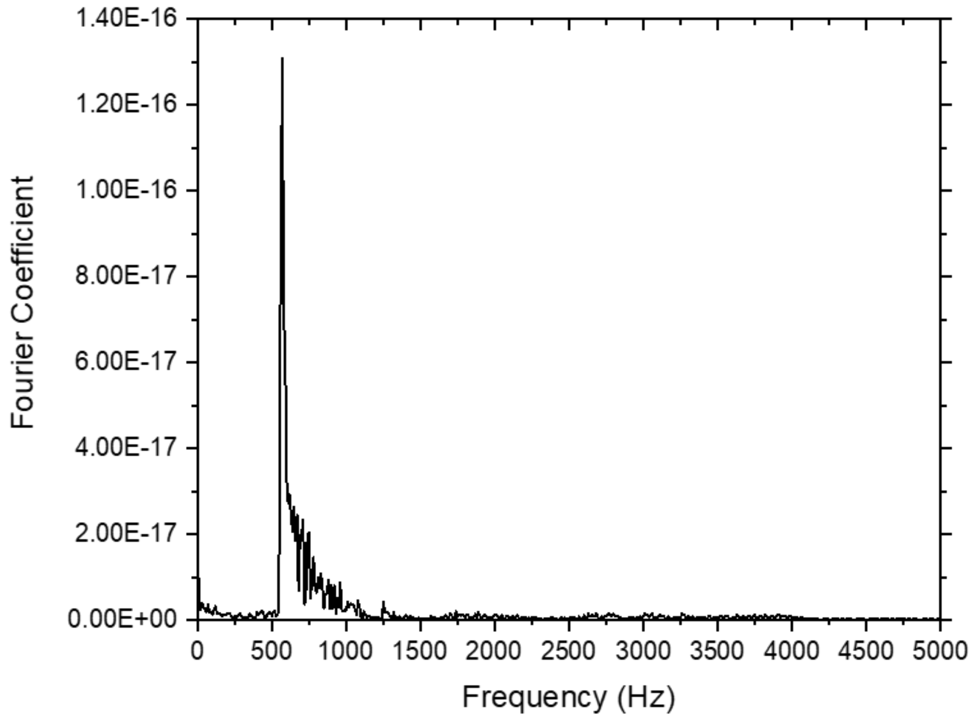

Figure 21: The out of plane displacement of the kagome strip at the detector from figure 18 transformed into the frequency domain through a Fourier transform.

Figures 20 and 21 demonstrate the kind of data that was collected from the strip models from the time dependent simulations. A comparison of the kagome, diamond, and mixed strip (figure 14) at N = 20 was performed through this method. A plain strip (figure 18) was also evaluated to act as a baseline for lattice comparison. Evaluating the time response of the kagome, diamond, mixed, and plain strip at the detector allowed for a comparison between the lattices. The comparison is shown in figure 22.

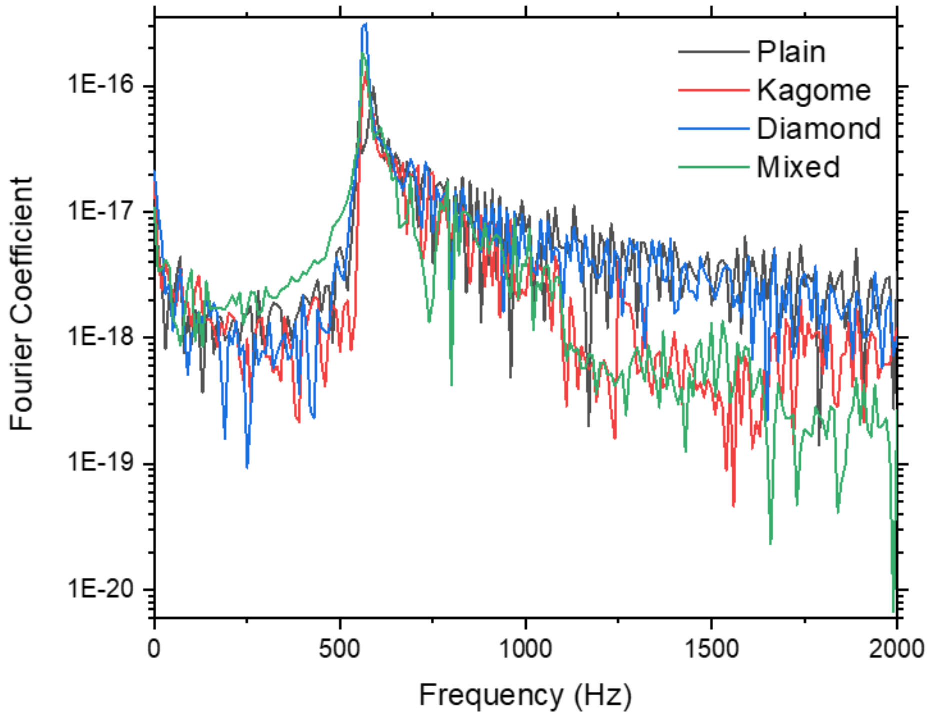

Figure 22: The frequency response for the out of plane displacement collected from the detector for the plain, kagome, diamond, and mixed strip at N = 20. A logarithm base 10 was implemented to the y-axis data for better illustration of each performance.

Plain	Kagome	Diamond	Mixed
1.411E-14	1.026E-14	1.793E-14	1.197E-14

Table 1: The results of the trapezoidal integral applied to the frequency response of the strips evaluated. The kagome strip had the lowest area under the curve which meant the most suppression observed.

Based on figure 22, it was immediately noticed that the diamond lattice strip was unsuccessful in suppressing higher frequencies (>1000Hz). There was much overlap between the diamond response and the plain strip response at these frequencies. The kagome and mixed lattice were successful however, in suppressing frequencies higher than

1000 Hz. It is suspect that a band gap may be present there for both lattices. At lower frequencies (i.e. 0 to 500 Hz), the mixed lattice underperformed compared to the kagome and diamond lattice. Furthermore, the area under each response was calculated using a trapezoidal integral function to determine which lattice performed best overall in terms of frequency suppression. In this case, the response with the lowest area would be the optimal lattice. For the N = 20 case, the kagome lattice out preformed both lattices as it had the lowest area under the curve. The mixed lattice was the second best to perform in terms of frequency suppression.

As shown in figures 21 and 22, it was apparent that the presence of a large frequency peak dominated all lattice and plain strip cases. This frequency peak had a frequency much lower than the impulse frequency set at 5000 Hz. It was suspected that due the nature of the cylinder, the frequency peak was caused by the ring mode of the cylinder. This frequency peak possessed a frequency near the ring frequency of the cylinder. This frequency has a large density of state which causes this distinguishable peak which indicates that it is a main vibrational signal perceived in a shock related event. Since all models were made highly parametric, further geometric manipulation was done on the strips which allowed for further testing to see if the peak could be suppressed. The kagome, diamond, and mixed lattice strips were evaluated at different N values to see if the dominant frequency peak could be suppressed through band gap manipulation.

As a subsequent step, the kagome, diamond, and mixed lattice strips were analyzed at different N values. These strips were evaluated at N = 12, 20, 36 for comparison. By changing the structure through changing the N unit cell value, the intent was to acquire more frequency suppression, especially at the frequency peak. Figures 23, 24, and 25 show the response calculated for the kagome, diamond, and mixed lattice strips, respectively.

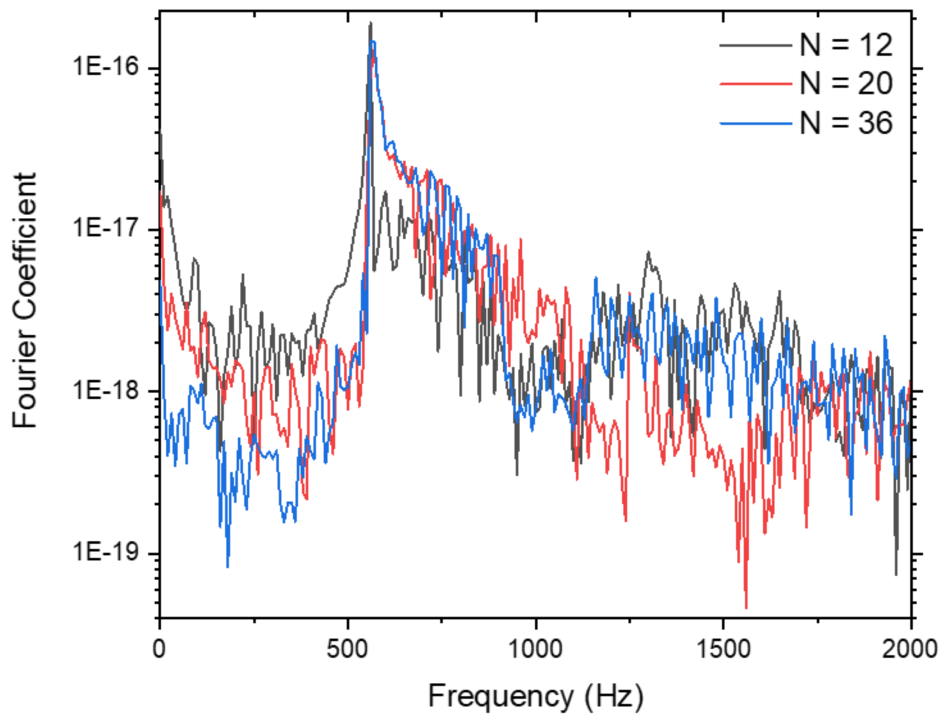

Figure 23: The kagome strip evaluated at different N values that correspond to the frequency domain of the out of plane displacement at the detector with a logarithm base 10 applied to the y-axis data.

N = 12	N = 20	N = 36
9.434E-15	1.026E-14	1.114E-14

Table 2: The results of the trapezoidal integral applied to the frequency response of kagome strips evaluated at different N values (i.e. 12, 20, 36). The N = 12 had the lowest area under the curve which meant the most suppression observed.

Figure 23 demonstrates the kagome lattice strip data evaluated at different N values. Regarding the structure, the higher the N value, the smaller the kagome unit cells will be since the space in which they are fitted in is fixed. For an N = 12 case, the kagome unit cells correspond to a much larger size since less unit cells are required to fit within the designated fixed space. With larger unit cells (i.e. N =12), the frequency suppression at lower frequencies (<500 Hz) was low compared to higher N values (i.e. N = 20 and 36). The highest suppression seen at these lower frequencies (<500 Hz) was for much smaller unit cells that corresponded to an N = 36 case. However, the N = 12 case did see the most suppression near the peak frequency when compared to the other two cases. At higher frequencies (>1000 Hz), neither extremes (i.e. N = 12 and 36) improved the suppression. The N= 20 case outperformed the other two case at these higher frequencies (>1000 Hz). Overall, it was observed for the kagome lattice that smaller unit cells work best in suppressing lower frequencies than larger unit cells.

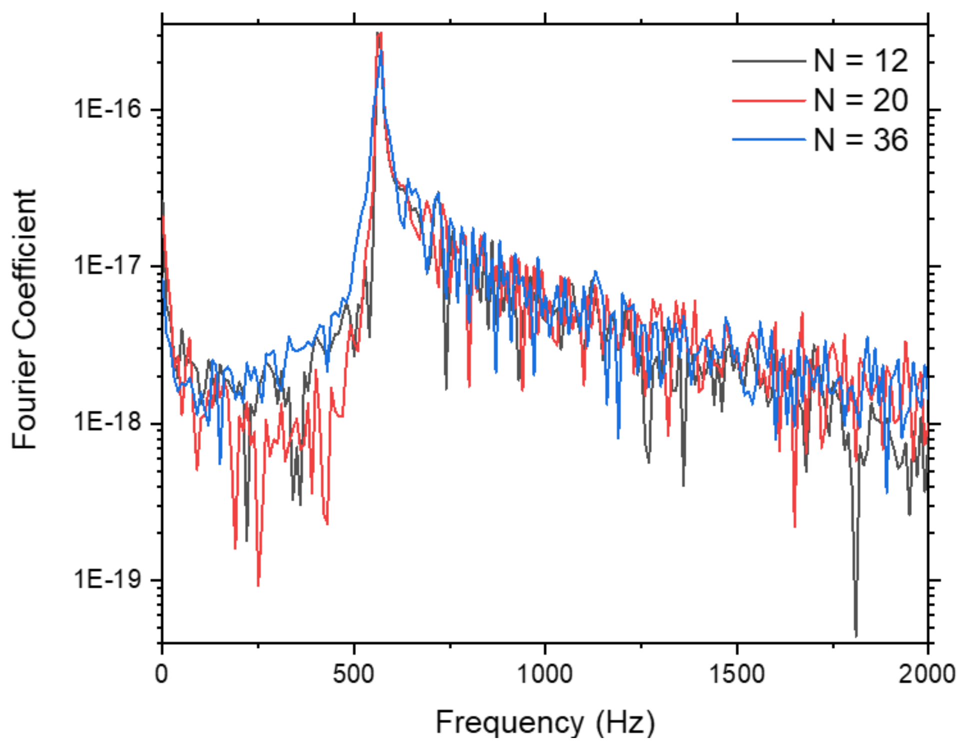

Figure 24: The diamond strip evaluated at different N values that correspond to the frequency domain of the out of plane displacement at the detector with a logarithm base 10 applied to the y-axis data.

N = 12	N = 20	N = 36
1.652E-14	1.793E-14	1.831E-14

Table 3: The results of the trapezoidal integral applied to the frequency response of diamond strips evaluated at different N values (i.e. 12, 20, 36). The N = 12 had the lowest area under the curve which meant the most suppression observed.

A similar analysis was done for the diamond lattice strip with varying N values as shown in figure 24. As shown in a previous comparison (i.e. figure 22), the diamond lattice provided little to no frequency suppression at higher frequencies (>1000 Hz). Its performance was comparable to a no lattice case (i.e. the plain strip) at these higher frequencies. This behavior was also demonstrated at varying N values. Increasing or decreasing the N value of the structure, thus changing the size of each unit cell, had little to no effect on frequency suppression at higher frequencies (>1000 Hz). However, unlike the kagome lattice, for a structure such as the diamond lattice, frequency suppression was improved with larger unit cells (i.e. smaller N values).

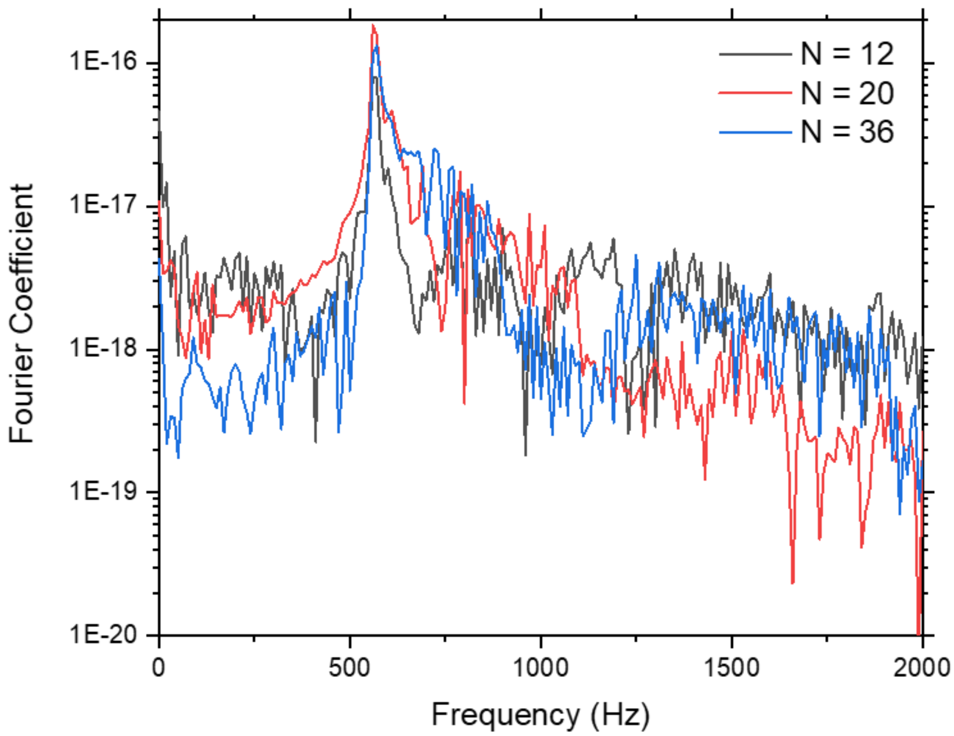

Figure 25: The mixed strip evaluated at different N values that correspond to the frequency domain of the out of plane displacement at the detector with a logarithm base 10 applied to the y-axis data.

N = 12	N = 20	N = 36
8.052E-15	1.197E-14	1.070E-14

Table 4: The results of the trapezoidal integral applied to the frequency response of mixed strips evaluated at different N values (i.e. 12, 20, 36). The N = 12 had the lowest area under the curve which meant the most suppression observed.

The mixed lattice strip analysis at varying N values is shown in figure 25. Like the kagome lattice, the mixed lattice had a similar behavior. At smaller N values (i.e. N =12 and 20), the frequency suppression was much lower at lower frequencies (<500 Hz) than that produced by a higher N value (i.e. N = 36). With smaller mixed unit cells, the frequency suppression at lower frequencies (<500 Hz) is greater than that produced by larger unit cells. With larger unit cells (i.e. N = 12) however, the suppression for frequencies near the ring frequency was much more than with any of the other cases. Furthermore, at higher frequencies (>1000 Hz), neither extremes (i.e. N = 12 and 36) improved the suppression by much like the kagome lattice. The N = 12 case demonstrated the most suppression at these higher frequencies.

Testing different N values within the lattice strips allowed for the evaluation of the behavior of these structures with changing unit cell sizes. For the case of the kagome and mixed lattice, it was apparent that smaller unit cells are better at suppressing lower frequencies (<500 Hz). However, these smaller unit cells provided very little improvement to the suppression of much larger frequencies (>1000 Hz). Larger unit cells, as seen in the case of N = 12, for the kagome and mixed lattice did show some improvement in suppressing the large frequency peak near the ring frequency of the cylinder. The overall structure of the diamond lattice proved to be inefficient in suppressing larger frequencies. Subsequent lattice evaluations were kept at N = 20 because this case proved to be effective in suppressing larger frequencies when compared to other N values. A comparison of the lattices for N =12 and 36 compared to a baseline in single plots are shown in the Appendix. An evaluation of combination lattices was done to see if it could outperform single lattice strips.

Combination lattices as described in chapter 3 were designed to see if further noise suppression could be obtained in the frequency domain when compared to single lattices. The hypothesis was that by having two mechanically contrasting lattices within the same structure, the structure would experience a similar behavior to acoustic impedance and further suppress any vibrations experienced by the lattice. The first set of cases considered were the half and half lattices. By half and half, it is meant that the array of unit cells within strip was comprised of half of one lattice and half of another as seen in figure 16. The first combination lattice analyzed was composed of the kagome lattice and the mixed lattice and the frequency data is shown in figure 26.

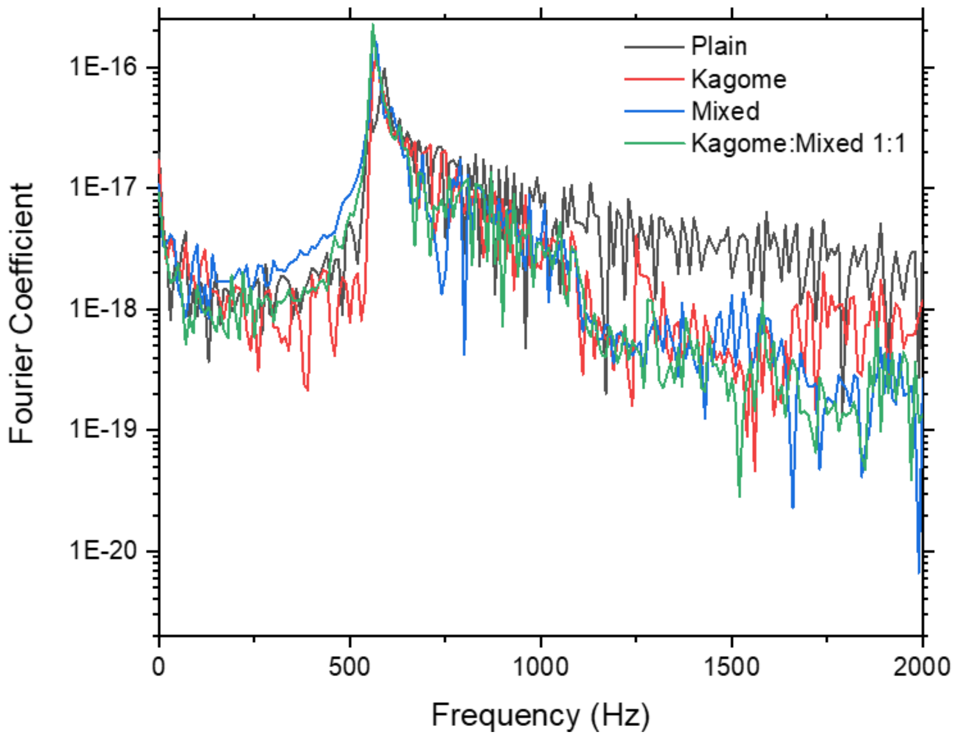

Figure 26: The half and half kagome and mixed strip data corresponding to the frequency domain from the out of plane displacement at the detector with a logarithm base 10 applied to the y-axis data. The single kagome and mixed lattice strip data was also included for comparison.

Plain	Kagome	Mixed	K:M 1:1
1.411E-14	1.026E-14	1.197E-14	1.134E-14

Table 5: The results of the trapezoidal integral applied to the frequency response of the plain, kagome, mixed, and the half and half kagome mixed strip. The kagome strip had the lowest area under the curve which meant the most suppression observed.

The half and half strip consisting of the kagome and mixed lattice (figure 16b) was analyzed and plotted as shown in figure 26. The single kagome strip still performed better overall in terms of frequency suppression when compared to the other two lattices. All strips considered still had a large frequency peak near the ring frequency of the cylinder from where they were cut from. Introducing two mechanically contrasting lattices within the same structure did not help suppress the frequency peak. However, at the higher frequencies (>1000 Hz), the half and half kagome and mixed strip demonstrated more suppression of noise in frequency domain than the single lattices did. Applying a trapezoidal integral function onto the area region that corresponds to frequencies greater than 1000 Hz demonstrated that the half and half strip possessed the least of amount of area. Hence, more suppression in the frequency domain. Within this space, the half and half kagome and mixed strip response had 37% less area than the single kagome strip response. Also, the half and half kagome and mixed strip response had 14% less area than the single mixed strip response.

The second half and half strip considered was the kagome and diamond strip as shown in figure 16a. The data collected and plotted from this case is shown in figure 27. As mentioned earlier, the diamond lattice provided little improvement at higher frequencies since its response was comparable to a no lattice case. However, the introduction of the kagome lattice improved its overall performance significantly at these higher frequencies. In terms of best suppression at frequencies greater than 1000 Hz, by applying the trapezoidal integral function, it was shown that both the kagome response and the half and half kagome and diamond response had almost identical area values. This indicates that the geometric shape of the kagome lattice improved the diamonds response to roughly to level of the kagome's frequency suppression for this range. In terms of low frequency ranges (<500 Hz), both single strip lattices outperformed the half and half lattice in terms of frequency suppression.

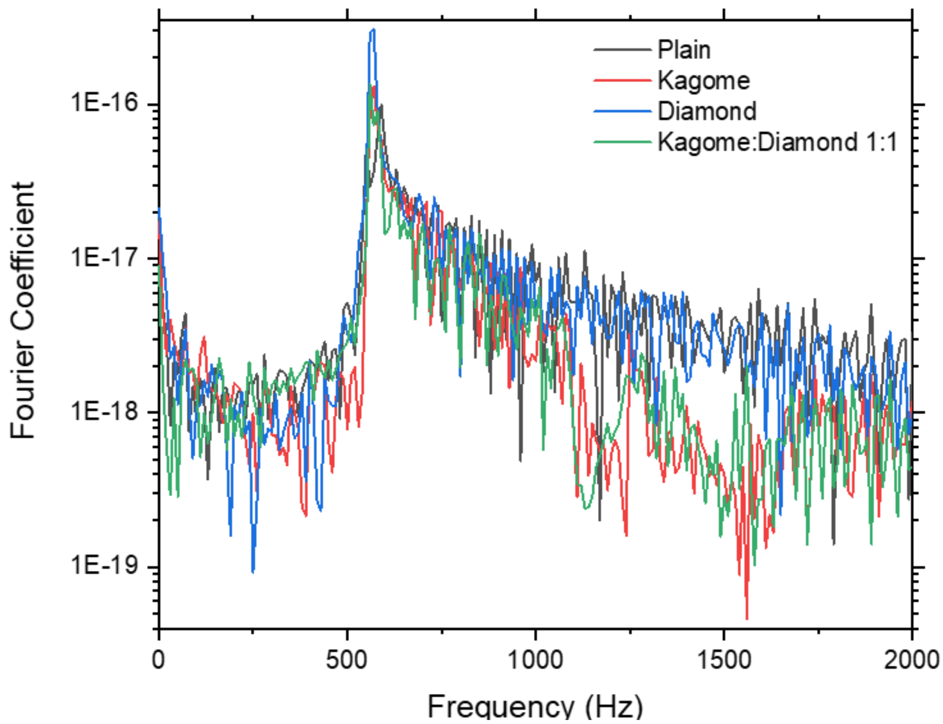

Figure 27: The half and half kagome and diamond strip data corresponding to the frequency domain from the out of plane displacement at the detector with a logarithm base 10 applied to the y-axis data. The single kagome and diamond lattice strip also included for comparison.

Plain	Kagome	Diamond	K:D 1:1
1.411E-14	1.026E-14	1.793E-14	9.313E-15

Table 6: The results of the trapezoidal integral applied to the frequency response of the plain, kagome, diamond, and the half and half kagome diamond strip. The half and half kagome diamond strip had the lowest area under the curve which meant the most suppression observed.

The last half and half strip analyzed consisted of the mixed and diamond lattice as shown in figure 16c. The frequency domain data was plotted and is shown in figure 28. In terms of low frequency ranges (<500 Hz), the diamond lattice still proved to be the most effective in attenuating that frequency noise. Furthermore, with regards to higher frequencies, an analysis of the area underneath the response demonstrated that the addition of the mixed lattice improved frequency suppression to the diamond's structure. The trapezoidal integral proved that more suppression was seen by the half and half mixed and diamond lattice when compared to its single lattice counterparts.

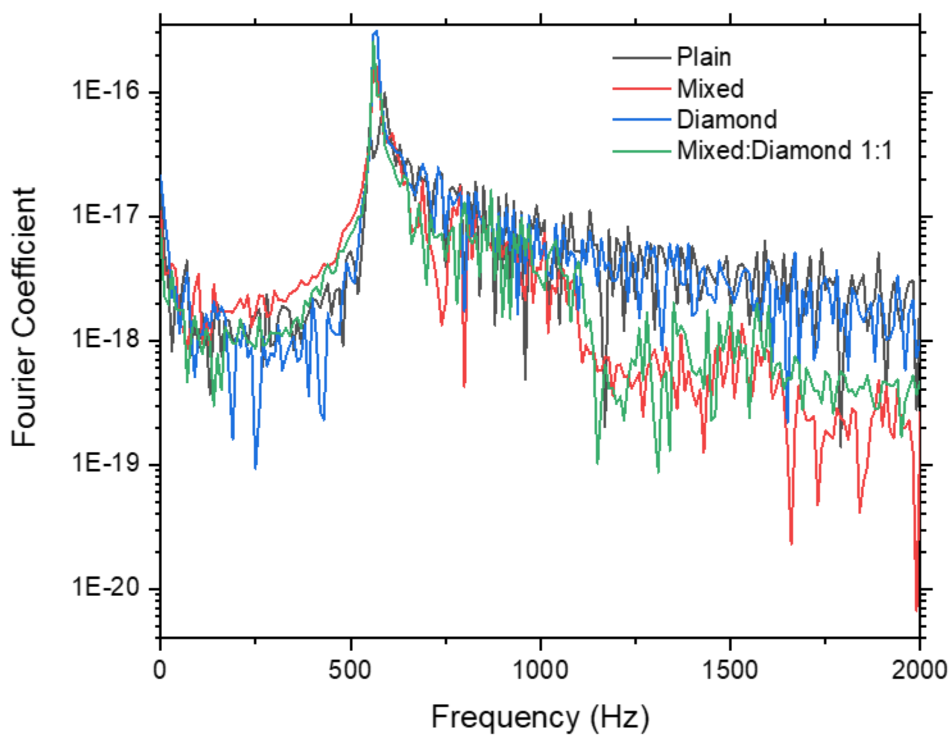

Figure 28: The half and half mixed and diamond strip data corresponding to the frequency domain from the out of plane displacement at the detector with a logarithm base 10 applied to the y-axis data. The single mixed and diamond lattice strip also included for comparison.

Plain	Diamond	Mixed	M:D 1:1
1.411E-14	1.793E-14	1.197E-14	1.133E-14

Table 7: The results of the trapezoidal integral applied to the frequency response of the plain, mixed, diamond, and the half and half mixed diamond strip. The half and half mixed diamond strip had the lowest area under the curve which meant the most suppression observed.

An alternative approach to the half and half strips were the lattice strips that contained alternating unit cells of different lattices within a strip. The first alternating unit cell strip evaluated was the kagome and mixed strip as shown in figure 17b. The frequency domain data is shown in figure 29. Initially, the kagome and mixed alternating strip outperforms their single strips counterpart in terms of frequency suppression from 0 to 500 Hz. The application of the alternating unit cells did not help suppress the frequency peak shown at 560 Hz. The alternating unit cell strip, however, did help improve the suppression of frequency at frequencies greater than 1000 Hz. An analysis of the area under each response demonstrated that the alternating unit cell response had the lowest area out all cases indicating an overall better suppression. The implementation of alternating unit cells for this case also established a band gap at roughly 1200 Hz.

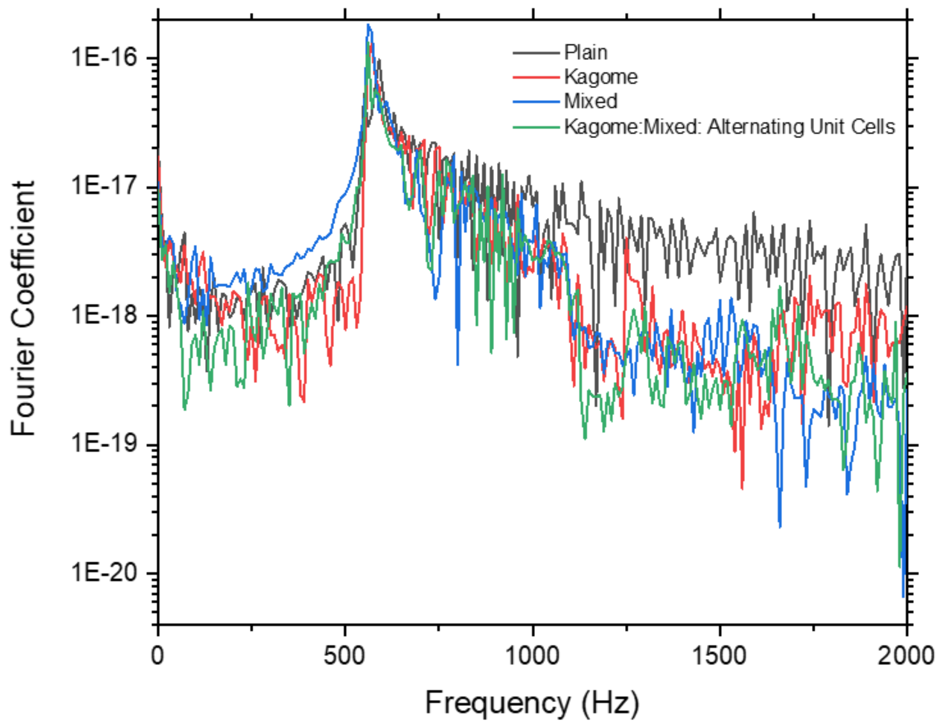

Figure 29: The kagome and mixed strip data consisting of alternating unit cells. The data corresponds to the frequency domain from the out of plane displacement at the detector with a logarithm base 10 applied to the y-axis data. The single kagome and mixed lattice strip also included for comparison.

Plain	Kagome	Mixed	K:M AUC
1.411E-14	1.026E-14	1.197E-14	8.688E-15

Table 8: The results of the trapezoidal integral applied to the frequency response of the plain, kagome, mixed, and the alternating unit cell kagome mixed strip. The alternating unit cell kagome mixed strip had the lowest area under the curve which meant the most suppression observed.

The second alternating strip analyzed was the kagome and diamond variation as shown in figure 17a. The frequency domain data was plotted and is shown in figure 30.

Once again, from frequencies ranging from 0 to 500 Hz, the alternating unit call strip, for this case, outperformed the single lattice strip counterparts. This was confirmed via the trapezoidal integral function applied to this range. Furthermore, for frequencies greater than 1000 Hz, the alternating unit cell strip did not assist as well as expected. Overall, more suppression was seen from kagome lattice strip than with the alternating strip. However, the application of alternating kagome and diamond unit cells narrowed the region where the peak frequency is dominant. This new periodicity introduced a band gap roughly at 750 Hz. In terms of overall suppression, the alternating strip here outperformed the single lattice strips.

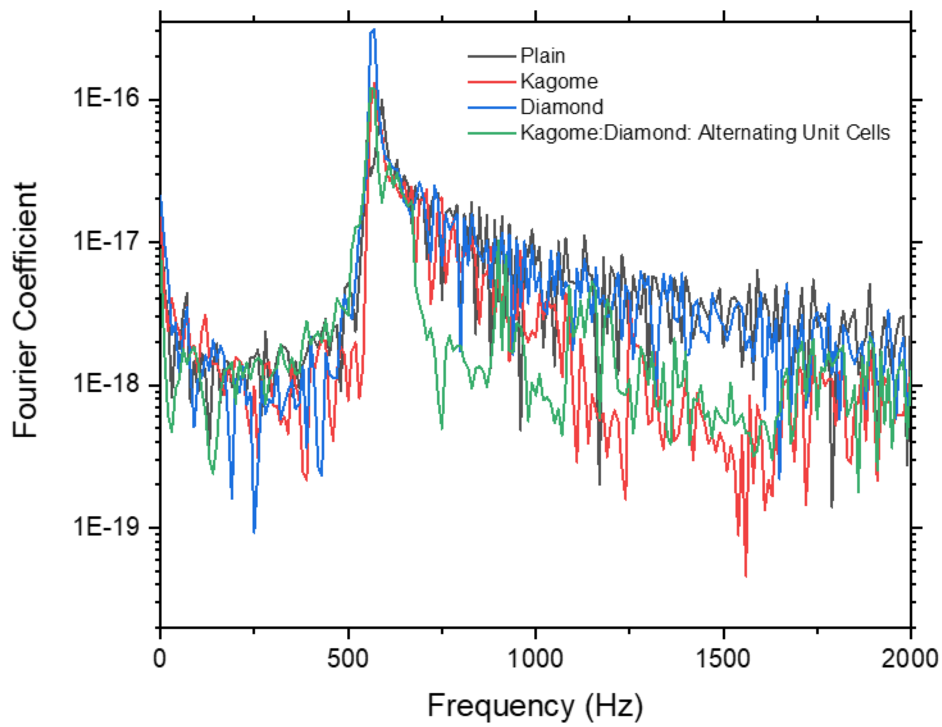

Figure 30: The kagome and diamond strip data consisting of alternating unit cells. The data corresponds to the frequency domain from the out of plane displacement at the

detector with a logarithm base 10 applied to the y-axis data. The single kagome and diamond lattice strip also included for comparison.

Plain	Kagome	Diamond	K:D AUC
1.411E-14	1.026E-14	1.793E-14	8.718E-15

Table 9: The results of the trapezoidal integral applied to the frequency response of the plain, kagome, diamond, and the alternating unit cell kagome diamond strip. The alternating unit cell kagome diamond strip had the lowest area under the curve which meant the most suppression observed.

The last alternating unit cell strip analyzed consisted of the mixed and diamond lattice as shown in figure 17c. The frequency domain data was plotted and is shown in figure 31. The alternating strip consisting of the mixed and diamond strip did not improve the suppression at lower frequencies (<500 Hz). In fact, the implementation of the mixed lattice adversely affected the diamonds ability to suppress low frequency noise. However, the alternating strip did improve the high frequency suppression at certain areas. For instance, this new periodicity introduced a new band gap at 1000 Hz where the individual mixed lattice failed to suppress. In terms of overall suppression, the alternating lattice strip here outperformed single lattice strip cases despite underperforming at lower frequencies.

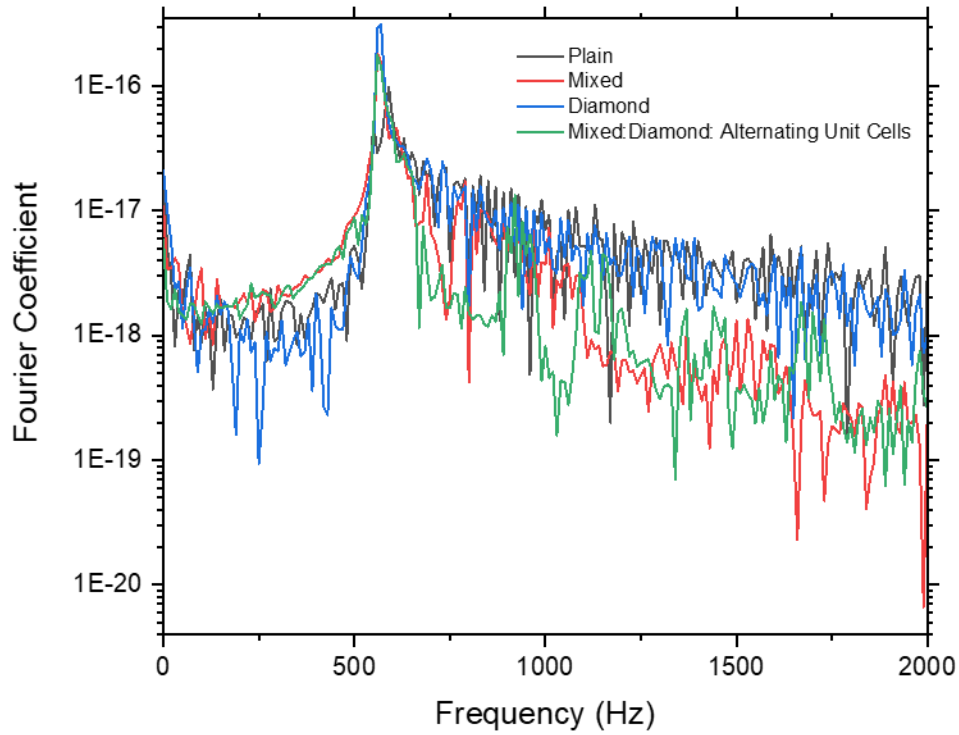

Figure 31: The mixed and diamond strip data consisting of alternating unit cells. The data corresponds to the frequency domain from the out of plane displacement at the detector with a logarithm base 10 applied to the y-axis data. The single mixed and diamond lattice strip also included for comparison.

Plain	Diamond	Mixed	M:D AUC
1.411E-14	1.793E-14	1.197E-14	1.031E-14

Table 10: The results of the trapezoidal integral applied to the frequency response of the plain, diamond, mixed and the alternating unit cell mixed diamond strip. The alternating unit cell mixed diamond strip had the lowest area under the curve which meant the most suppression observed.

Introducing two different lattice structures within the same geometry improved the overall suppression seen with the individual lattice strips. By having two mechanically contrasting lattices within the same structure, an acoustic impedance effect occurs, and further band gaps were introduced as seen in the previous plots. Apart from the kagome and mixed half and half lattice strip (figure 16b), all cases demonstrated that they have an overall better suppression ability than their individual lattice counterparts. A comparison between the half and half strips and the alternating unit cells strip was performed to see which lattice strip would perform the best overall. Figures 32 and 33 show the half and half and alternating unit cell strip comparison, respectively.

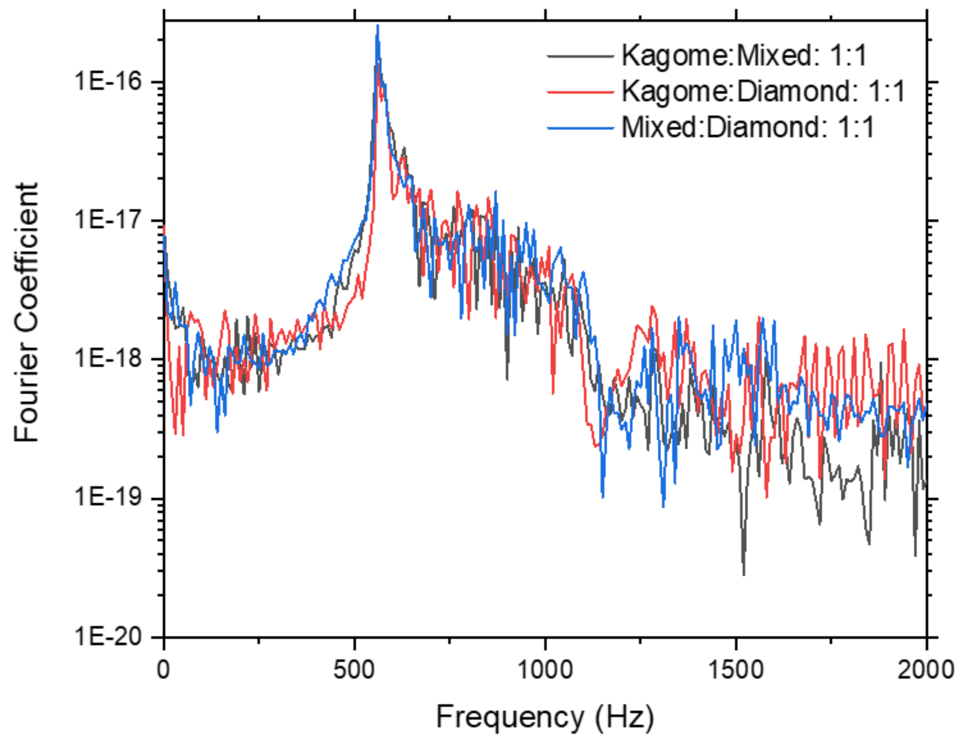

Figure 32: All half and half cases analyzed for an N = 20 case.

K:M 1:1	K:D 1:1	M:D 1:1
1.134E-14	9.313E-15	1.133E-14

Table 11: The results of the trapezoidal integral applied to the frequency response of the all the half and half strips evaluated (i.e. kagome mixed (K:M 1:1), kagome diamond (K:D

1:1), and mixed diamond (M:D 1:1)). The half and half kagome diamond strip had the lowest area under the curve which meant the most suppression observed.

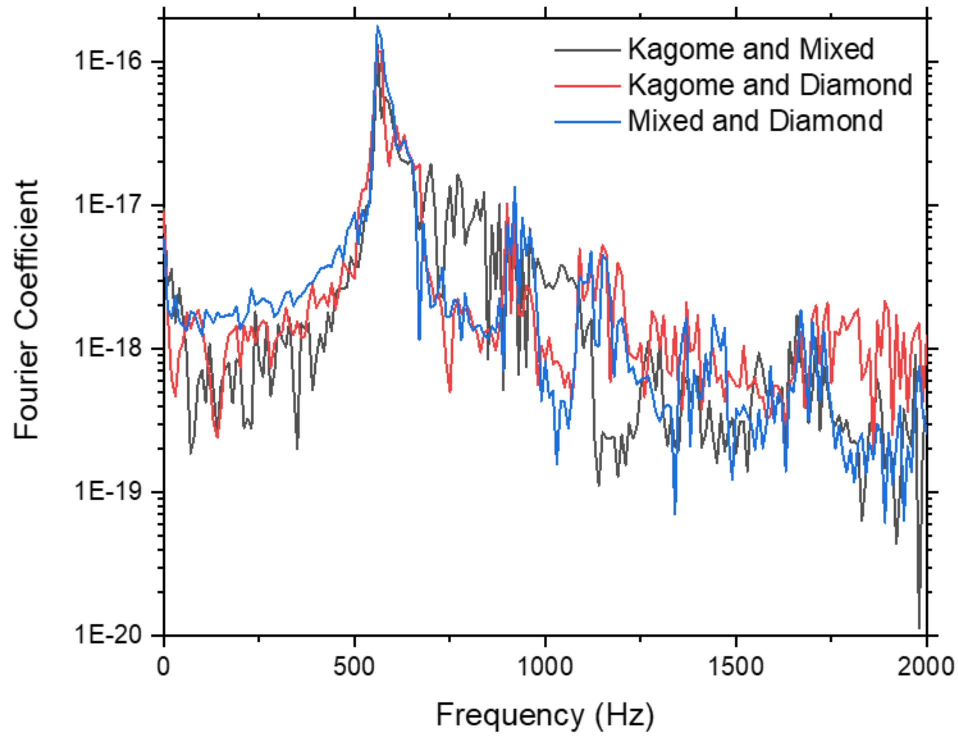

Figure 33: All strips with alternating unit cell cases analyzed for N = 20.

K:M AUC	K:D AUC	M:D AUC
8.688E-15	8.718E-15	1.031E-14

Table 12: The results of the trapezoidal integral applied to the frequency response of the all the alternating unit cell strips evaluated (i.e. kagome mixed (K:M AUC), kagome diamond (K:D AUC), and mixed diamond (M:D AUC)). The alternating unit cell kagome mixed strip had the lowest area under the curve which meant the most suppression observed.

For the cases involving the half and half strips, in terms of overall best frequency suppression, the kagome and diamond half and half strip performed the best. This has demonstrated that the addition of the diamonds ability to suppress low frequencies and the ability of the kagome lattice to suppress higher frequencies was optimal for overall suppression. Furthermore, regarding the alternating unit cell strips, the kagome and mixed variation performed the best overall. When comparing both best case scenarios, the kagome and mixed variation of alternating unit cells was the overall best in frequency suppression for all the strips considered. Though introducing a different lattice within the same structure helped improve the overall suppression of noise experienced by the detector, a large frequency peak was still dominant in all cases.

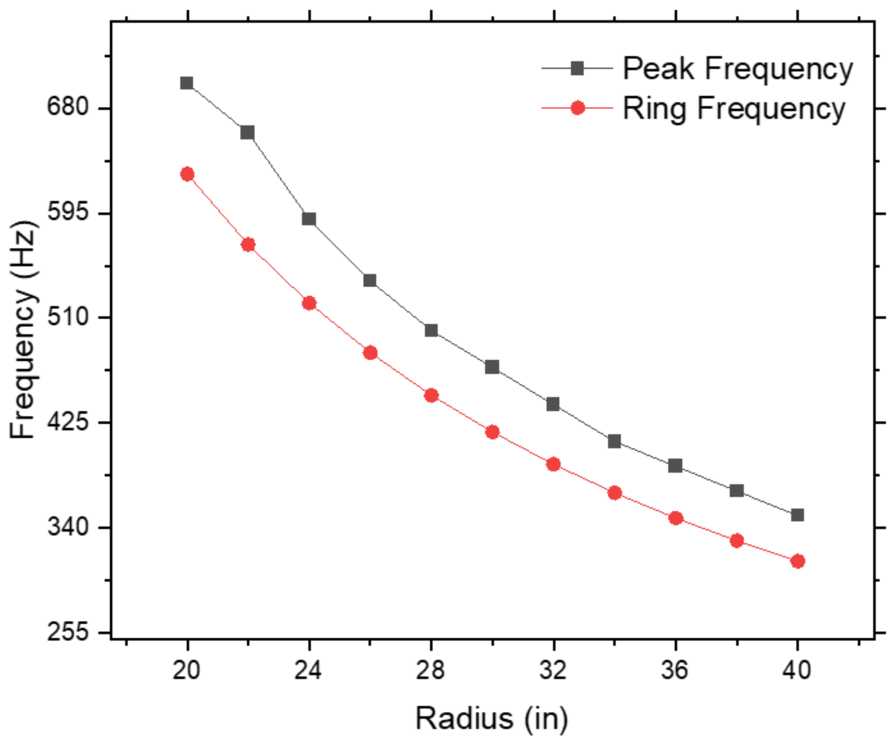

Figure 34: The theoretical ring frequency calculated for a cylindrical shell with the kagome lattice implemented at different radiuses. The resultant peak frequency from the resultant frequency domain plots is also included.

Each strip case evaluated had a large frequency peak near the ring frequency of the cylindrical shell. This was suspected to be a behavior caused the cylindrical geometry from which the strips are cut from. To evaluate the behavior of this frequency peak, a parametric sweep of the radius was performed on the individual kagome lattice strip. The results from the parametric sweep of the cylindrical shell radius is shown in figure 34. From the frequency domain results from each simulation, the peak frequencies were collected at their respective radiuses. The range of radiuses evaluated spanned from 20 to 30 inches in increments of 2 inches. The theoretical ring frequency of the cylindrical shell with a kagome lattice implemented was calculated with the following equation.

$$f_r = \frac{c_L}{2\pi r} \tag{4.1}$$

Where c_L is the longitudinal wave speed calculated by equation 2.10 and r is the radius of the cylinder. The longitudinal wave speed depended on the lame parameters of the structure, mainly λ and μ. The lame parameters λ and μ were calculated using equations 2.7 and 2.8, respectively.

Since the kagome lattice was implemented to the overall cylindrical shell structure, using equations 2.7 and 2.8 to find λ and μ required the use the effective properties of the kagome lattice. The effective properties of the kagome lattice depended on the lattice material and the filling fraction. The filling fraction, denoted by α, was determined to be roughly 0.2 and is described by the following equation.

$$\alpha = \sqrt{3}\,\frac{t}{b} \tag{4.2}$$

Where t is the thickness of the bars the make up the kagome lattice, and b is the length of one of the triangles that make up the kagome unit cell. A good approximation of the effective properties is described by the following equations.

$$E^* = \frac{\alpha}{3} E_o \tag{4.3}$$

$$\nu^* = \frac{1}{3} \tag{4.4}$$

Where E^* is the effective modulus, E_o is the bulk modulus of the material, and ν^* is the effective Poisson ratio of the kagome lattice. Implementing the effective properties into equations 2.7 and 2.8 allowed for the calculation of the theoretical ring frequency.

The dominant peak present in all strip cases evaluated in the frequency domain was seen to be near the ring frequency of the cylinder. The behavior of this peak was confirmed to be dependent on the diameter of the cylinder as shown in figure 34. Figure 34 confirms that the peak frequency follows the same trend as the ring frequency does with changing diameters. In a collaborative effort with another research group led by Dr. Andrew Norris of Rutgers University, the peak frequency in the kagome strip could be suppressed using low frequency cantilevers. This low frequency cantilever approach essentially creates local resonators within each kagome unit cell that are tuned to the ring frequency of the structure. Essentially by tuning these cantilevers to the appropriate ring frequency, they act as resonators and trap energy from the ring mode. Figure 35 shows the tuned cantilevers attached the kagome unit cells in a strip cut from a cylindrical shell.

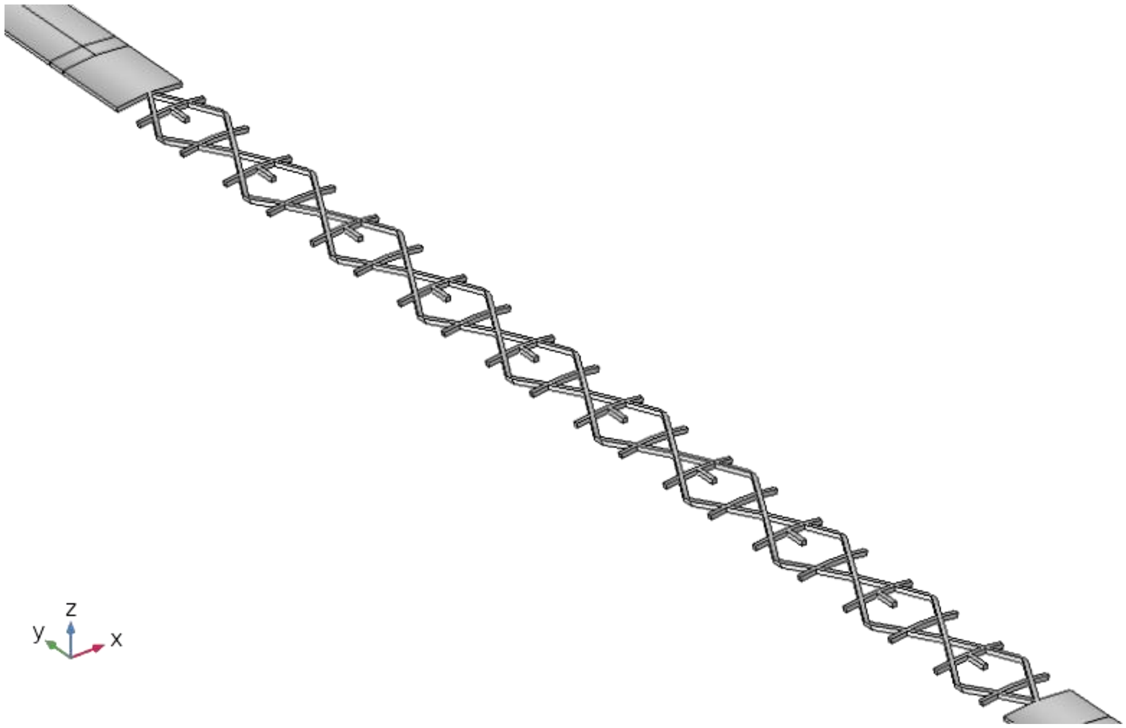

Figure 35: Cantilever resonators tuned to the frequency of the ring mode of the cylinder attached to the kagome lattice strip.

Figure 35 demonstrates the tuned low frequency cantilevers coupled with the kagome lattice strip. The kagome lattice strip with the cantilevers were simulated the same way as the previous strips were. The time domain solutions were converted to the frequency domain through a Fourier transform. The frequency domain data are shown in figures 36 and 37, respectively. Figures 36 and 37 demonstrate the frequency domain response of the kagome lattice strip with and without the cantilevers for comparison. Both figures 36 and 37 are the same plots, however figure 37 has a logarithm base 10 applied to its y-axis data.

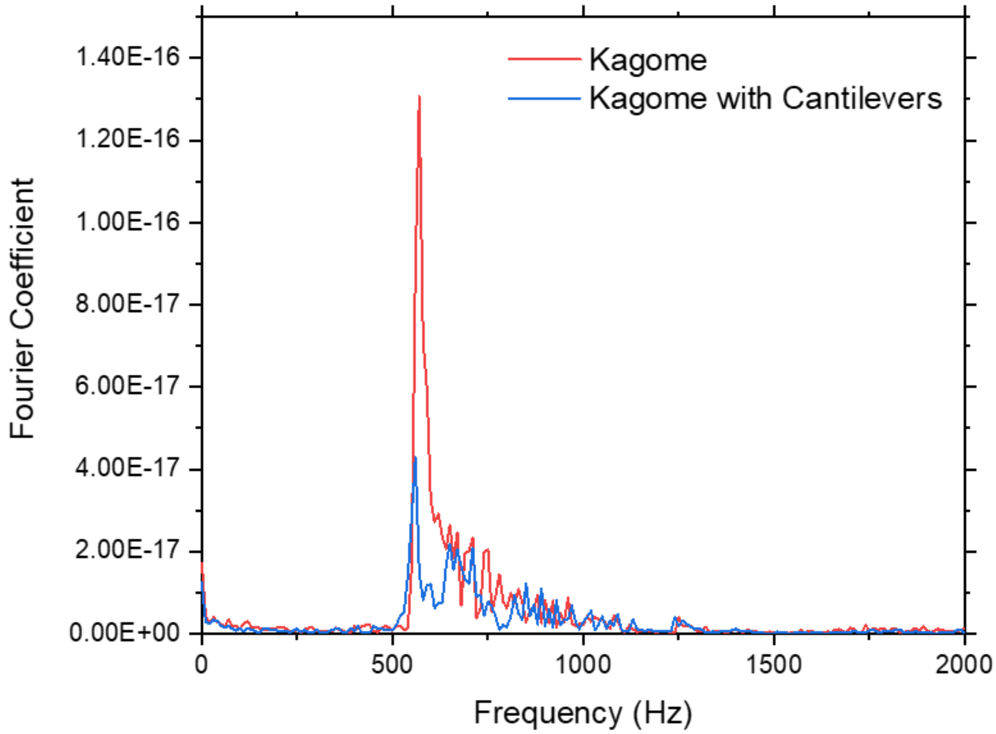

Figure 36: The frequency response of the kagome lattice with the tuned cantilever resonators along with the non-cantilever case.

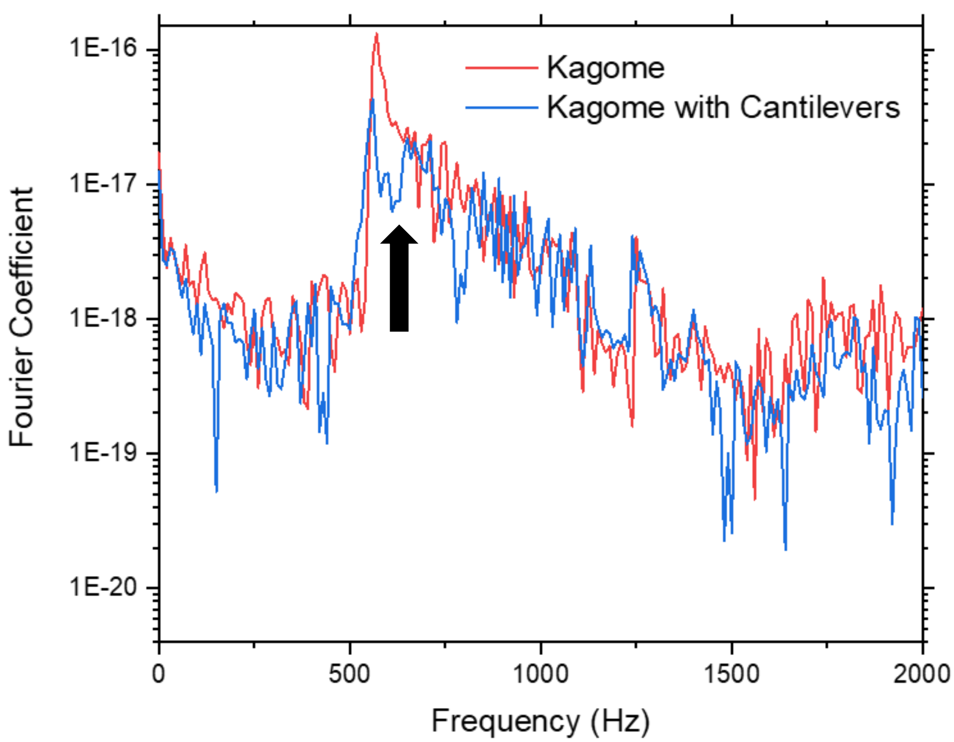

Figure 37: The frequency response of the kagome lattice with the tuned cantilever resonators along with the non-cantilever case with a logarithmic base 10 applied to the y-axis data.

The evaluation of the kagome lattice with the low frequency cantilevers instantly demonstrated that most of the ring mode energy is being trapped by these cantilevers during propagation. The peak from kagome lattice response dropped by a factor 3 with the cantilevers when compared to the original kagome lattice strip response. A screenshot of the kagome lattice strip with the cantilevers during the pulse shows that most of the energy is being trapped within the first unit cell cantilever as shown in figure 38. The first unit cell being the one closest to the source where the pulse is being applied. The first cantilever received the highest out of plane displacement out all the other cantilevers. A point probe was placed at the ends of the first, middle (5th), and last (10th) unit cell cantilever to compare the out of plane displacements in the time domain to prove this. Figure 39 shows that the first cantilever has significantly more displacement experienced than the 5th and 10th cantilever.

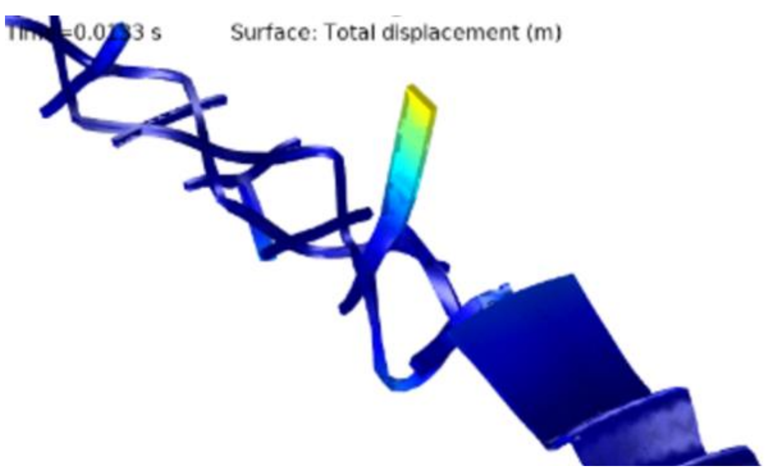

Figure 38: The kagome lattice with the low frequency cantilevers subjected to the half sine pulse at 0.0133s. The image shows the strip being near the source where the source is applied.

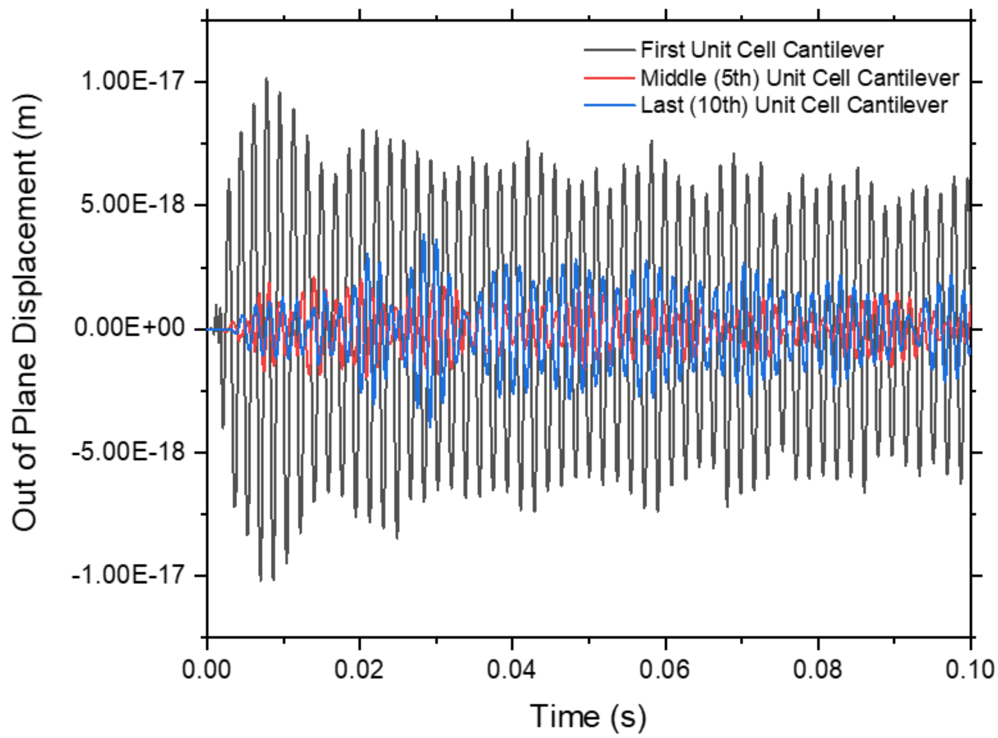

Figure 39: The out of plane displacement comparison for different cantilevers within the kagome lattice strip at N = 20.

With the success of the low frequency cantilevers in suppressing some of the ring mode energy of the structure, the next step was to implement a skin to the exterior. The purpose of the lattice is to suppress vibrations that may adversely affect the payload of the launch vehicle. A skin applied to the exterior, not only provides some protection, but allows for the lattice to be more aerodynamic during flight. To begin a 1.5 mm skin was applied to exterior of the kagome lattice strip with the cantilevers, as shown in figure 40. The roller boundary condition was applied to the sides of the skin also to ensure that it behaved like the lattice strip in a cylindrical body. Lastly, the infinite domains were applied to the ends of the strip also, identical to the lattice strip, to ensure no reflections from propagating waves.

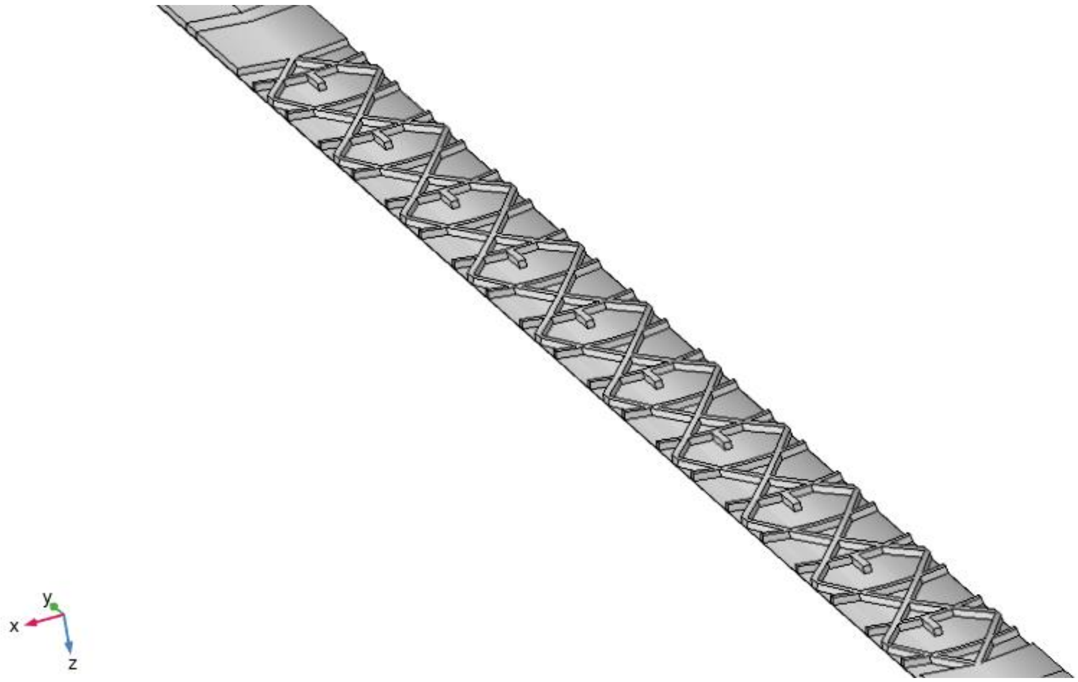

Figure 40: The kagome lattice strip with a 1.5 mm skin on the exterior for an N = 20 case.

A comparison of the kagome lattice strip with the low frequency cantilevers with and without the 1.5 mm skin was performed to evaluate the overall effect that the skin imposes. The frequency domain data for this analysis was plotted and is shown in figure 41. The addition of the 1.5 mm skin adversely affected the overall frequency suppression when compared the case where no skin is applied. Applying the trapezoidal integral function to both responses shows that the kagome lattice with just the cantilevers overall performs better than with the addition of the skin. Additionally, the implementation of a skin also increased the amplitude of dominant peak as seen before. It seems that the ring mode energy from the skin is contributing the energy experienced by the detector. Hence, allowing the peak frequency near the ring frequency to remain dominant again. The addition of the skin did, however improve suppression at higher frequencies such as at 750 and 1000 Hz when compared to a no skin case.

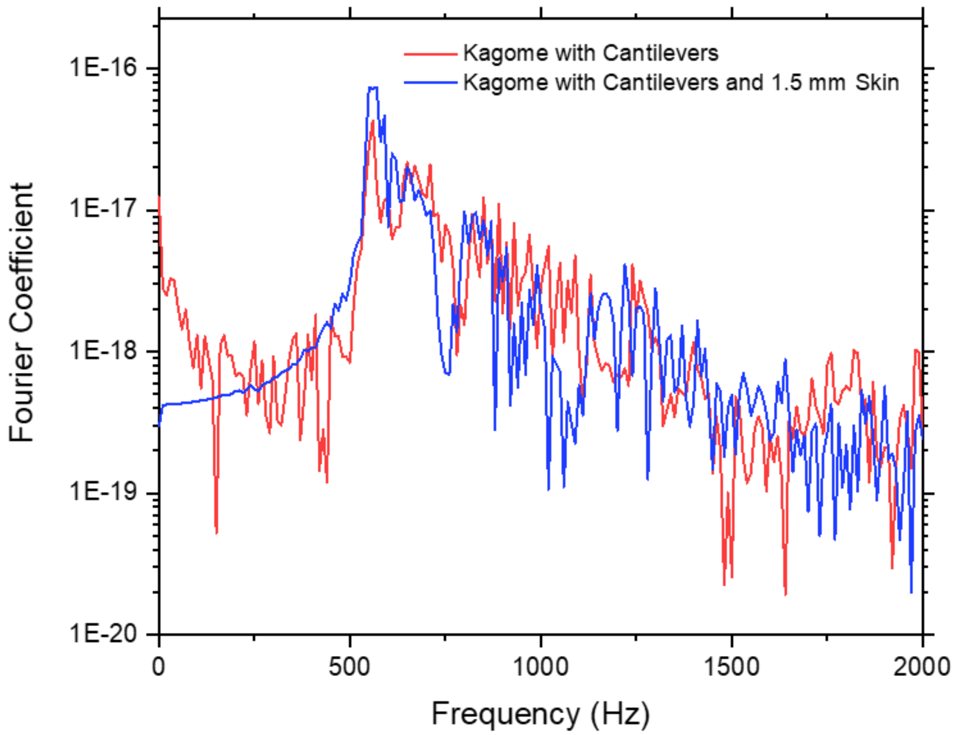

Figure 41: A comparison of the kagome lattice strip with the low frequency cantilevers with and without the 1.5 mm skin.

Kagome with Cantilevers (No Skin)	Kagome with Cantilevers (1.5mm Skin)
5.894E-15	7.304E-15

Table 13: The results of the trapezoidal integral applied to the frequency response of the kagome strip with cantilevers and no skin and the kagome strip with cantilevers and a 1.5 mm skin. The kagome strip with cantilevers and no skin performed the best in terms of suppression.

To get a sense of how the response behaves when manipulating the skin, the skin was increased in thickness to 5 mm. The response for a 5 mm skin on the kagome lattice with cantilevers is shown in figure 42. As expected, increasing the thickness of the skin negatively affects the overall suppression experienced by the detector. Not only that, with more bulk, the ring mode energy of the skin contributes more to the dominant peak seen near the ring frequency of the structure. The dominant peak with a thicker skin is roughly half a magnitude higher than the peak of thinner skin. Frequency suppressions seen at 750 and 1000 Hz are not as prominent as they used to be with the 5 mm skin. Overall, adding more bulk to the skin, negatively affects the frequency suppression especially at the dominant frequency peak.

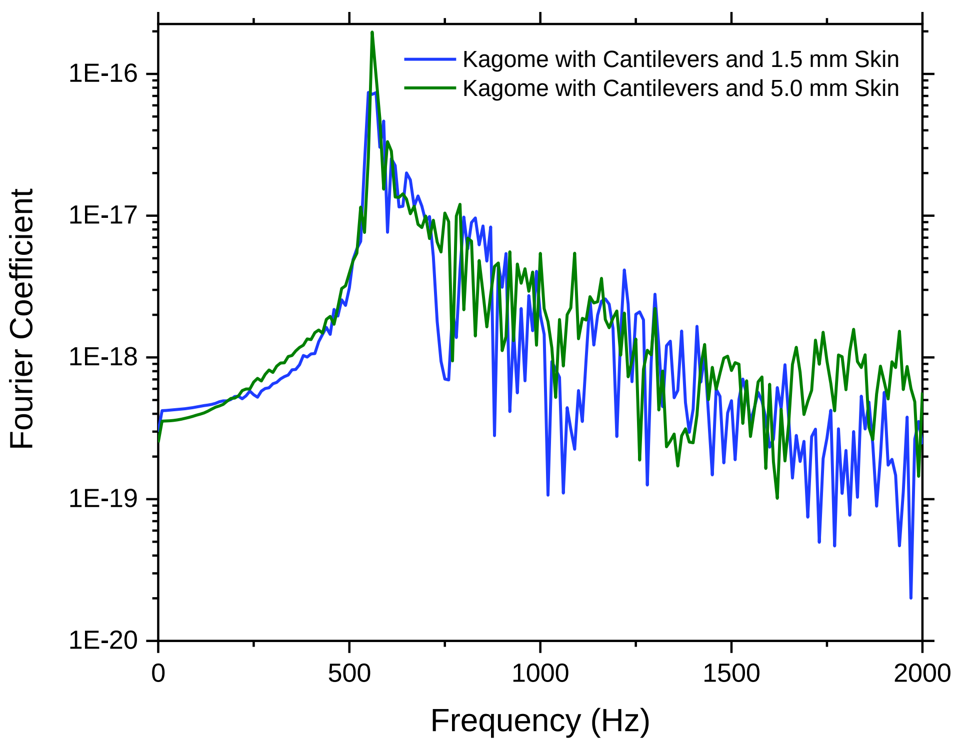

Figure 42: A comparison of the kagome lattice strip with the low frequency cantilevers with 1.5 mm skin and a 5 mms skin.

Kagome with Cantilevers (1.5mm Skin)	Kagome with Cantilevers (5.0mm Skin)
7.304E-15	8.707E-15

Table 14: The results of the trapezoidal integral applied to the frequency response of the kagome strip with cantilevers and a 1.5 mm skin and the kagome strip with cantilevers and a 5.0 mm skin. The kagome strip with cantilevers and a 1.5 mm skin performed the best in terms of suppression.

Knowing that adding more bulk to the skin contributes to more ring mode energy escaping the cantilevers, the skin was kept at 1.5 mm. To get an idea if the cantilevers were at all helping with the frequency suppression with the skin, a 1.5 mm skin was applied to the kagome lattice strip with no cantilevers for comparison. Figure 43 shows the result of this comparison. Based on figure 43, the cantilevers are still managing to trap some of the energy from the ring mode, but not as much as before. The peak for the case with the cantilevers is lower than that of the case without the cantilevers. In terms of overall suppression, the case with the cantilevers still outperforms the case without.

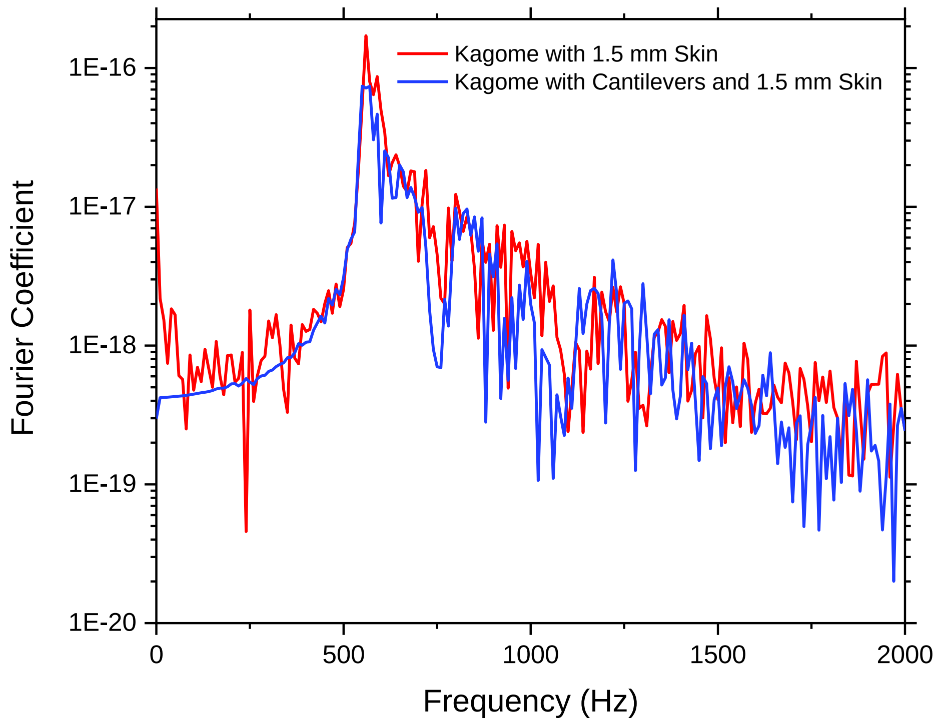

Figure 43: A comparison of the kagome lattice strip with and without the low frequency cantilevers with 1.5 mm skin on both cases.

Kagome with No Cantilevers (1.5mm Skin)	Kagome with Cantilevers (1.5mm Skin)
1.052E-14	7.304E-15

Table 15: The results of the trapezoidal integral applied to the frequency response of the kagome strip with no cantilevers and a 1.5 mm skin and the kagome strip with cantilevers and a 1.5 mm skin. The kagome strip with cantilevers and a 1.5 mm skin performed the best in terms of suppression.

It was suspected that most of the ring mode energy was trapped in the cantilevers through the displacement of the cantilevers as seen in figure 38. However, with the addition of skin, the cantilevers were coupled to the skin and thus not allowed to displace as much as before. Hence, not allowing the trapping of the ring mode energy and resulting a prominent frequency peak again. For the subsequent step, the idea was to decouple the cantilevers in increments of 0.25, 0.50, and 0.75 times their original thickness to allow for more displacement experienced by the cantilevers. By shortening the thickness, the hope was to allow the cantilevers to displace more, trap some of the ring mode energy and thus suppress the dominant peak. The results from this analysis are shown in figure 44.

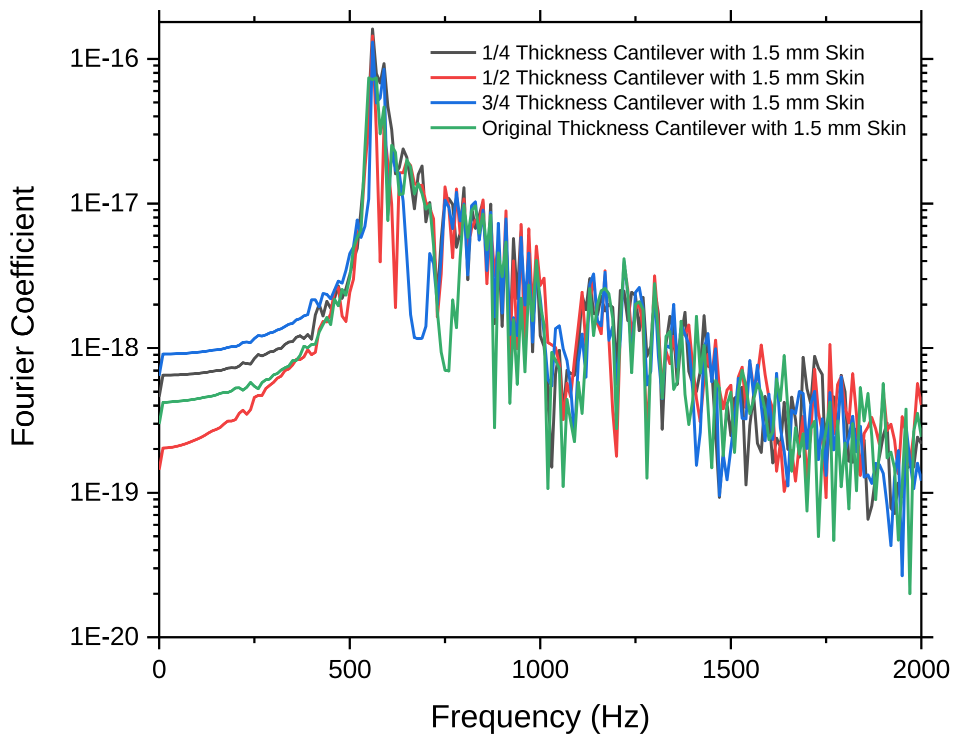

Figure 44: Varying the thickness of the cantilevers with the kagome lattice strip while having a 1.5 mm skin.

1/4 Thickness Cantilever (1.5 mm Skin)	1/2 Thickness Cantilever (1.5 mm Skin)	3/4 Thickness Cantilever (1.5 mm Skin)	Full Thickness Cantilever (1.5 mm Skin)
1.017E-14	7.273E-15	7.526E-15	7.273E-15

Table 16: The results of the trapezoidal integral applied to the frequency response of the kagome strip with its cantilevers decoupled from a 1.5 mm skin at ¼ of its original thickness, ½ of its original thickness, ¾ of its original thickness, and at its original

thickness. The kagome strip with cantilevers reduced to ½ of its original thickness preformed the best overall in terms of frequency suppression.

Decoupling the cantilever from the skin, did not prove effective in suppressing the dominant frequency peak. Reducing the thickness of the cantilever in increments of 0.25, 50, and 0.75 demonstrated little to no improvement at higher frequencies (>1000 Hz). The dominant peak near the ring frequency of the cylinder was not changed with decreasing thickness. A new band gap was established at roughly 750 Hz however, when reducing the thickness of the cantilever to ¾ of its original size. Furthermore, reducing the thickness of the cantilever to ½ of its original size, also manages to outperform the other cases at low frequency ranges (<500 Hz). Since decoupling the cantilever alone proved ineffective in suppressing the dominant peak experienced at 560 Hz, the cantilevers were re-tuned to the ring frequency with an eigenfrequency analysis. A specific case was considered for the re-tuning and that was at a cantilever thickness of ½ its original size. The idea of decoupling the cantilevers from the skin was still explored with this re-tuning.

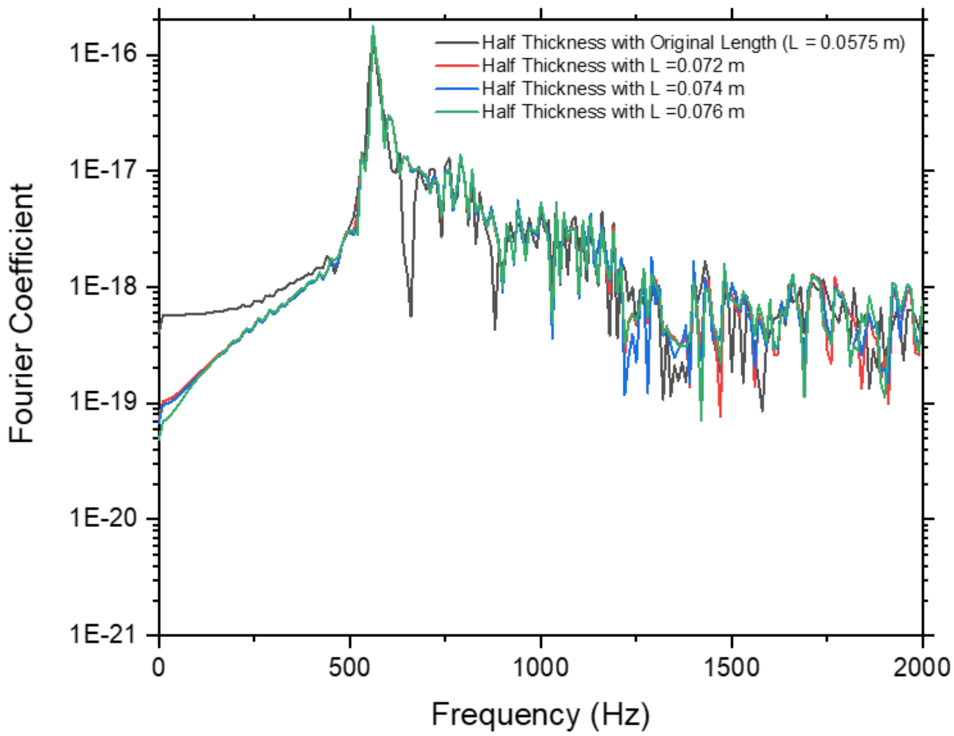

Figure 45: Varying the length of the cantilevers with the kagome lattice strip while having a 1.5 mm skin at ½ the original thickness of the cantilevers.

1/2 Thickness Cantilever (L = 0.0575m)	1/2 Thickness Cantilever (L = 0.0720m)	1/2 Thickness Cantilever (L = 0.0740m)	1/2 Thickness Cantilever (L = 0.0760m)
7.273E-15	8.344E-15	8.370E-15	8.343E-15

Table 17: The results of the trapezoidal integral applied to the frequency response of the kagome strip with its cantilevers decoupled from a 1.5 mm skin at ½ of its original thickness at varying lengths. The kagome strip with cantilevers reduced to ½ of its original thickness and kept its original length preformed the best overall in terms of frequency suppression.

The cantilevers were tuned to match the ring frequency of the structure while having half of its original thickness. By halving the thickness, the cantilevers would still be allowed to displace during propagation. Tuning this new cantilever with an eigenfrequency analysis resulted in a new cantilever length of 0.074 m. A parametric study of lengths close to this length was preformed to see if a behavior could be established. The results of the parametric study are shown in figure 45. When comparing the results to the cantilever with its original length at half its original thickness, the increase in cantilever length proved ineffective in suppressing the dominant frequency peak. All case had similar performance when dealing with higher frequencies (>1000 Hz). The increase in cantilevers did, however, improve the frequency suppression at a lower frequency range (<500 Hz).

It became apparent that the introduction of the skin and the decoupling of the cantilevers from the skin proved ineffective at trapping some of the ring mode energy. Currently, the best-case scenario is the kagome strip with the cantilevers implemented without the skin. This case however, only had cantilevers applied to the unit cells within the array that made up the strip. Simulating these low frequency cantilevers as if they were applied at every cell as shown in figure 46, demonstrates significant noise reduction in the frequency domain near the ring frequency due to the multiple cantilever coupling. A comparison of the kagome strip without the cantilevers, the kagome strip with the cantilevers only applied to the strip, and the kagome strip with the cantilevers applied to every cell is shown in figure 47. Future work will look at this implementation and see if a thinner skin could be applied without losing the cantilever’s ability to suppress some of the ring mode energy.

Figure 46: The kagome lattice strip at N = 20 with the low frequency cantilevers simulated as if these cantilevers were applied at every cell within the cylindrical shell with no skin.

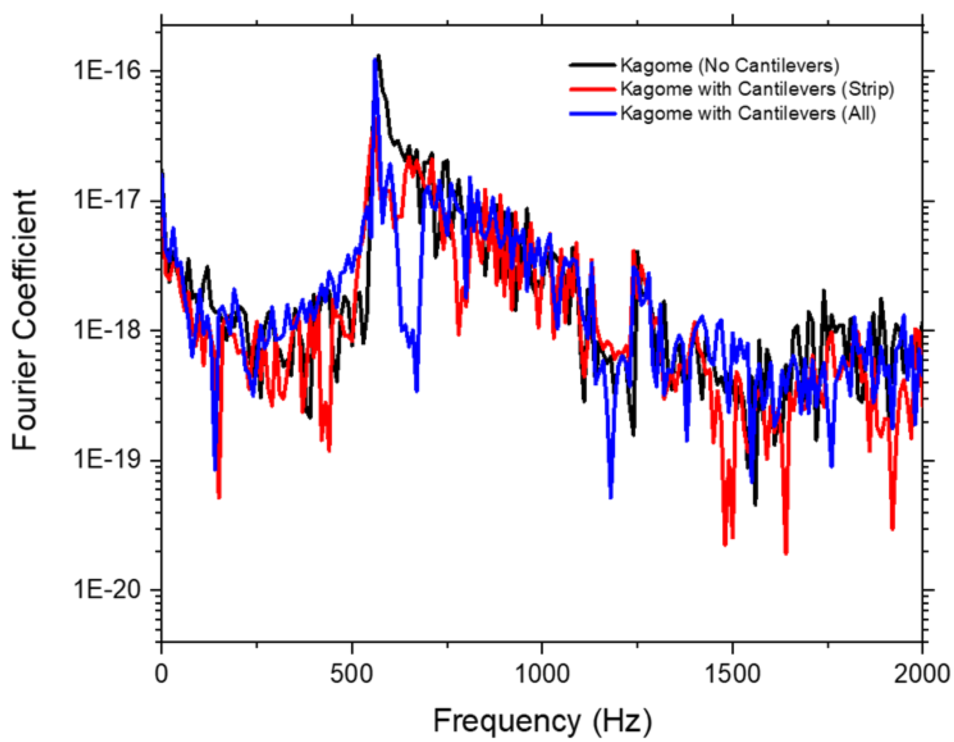

Figure 47: A comparison of the kagome strip without the cantilevers, the kagome strip with the cantilevers only applied to the strip, and the kagome strip with the cantilevers applied to every cell for an N = 20 case and no skin.

CHAPTER 5

CONCLUSION AND FUTURE WORK

With the evaluation of single lattice strips, it was determined that the kagome lattice outperformed the diamond and mixed lattice in terms of noise suppression detected by the detector for an N = 20 case. Both the kagome and mixed lattice exhibited the same behavior in that their smaller unit cells (i.e. N = 36) are better at suppressing lower frequencies (<500 Hz) than larger unit cells (i.e. N = 12). Meanwhile, larger kagome and mixed unit cells (i.e. N = 12) are better at suppressing larger frequencies (>1000 Hz). Larger kagome and mixed unit cells are especially better at suppressing some of the large frequency peak seen near the ring frequency of the structure. Apart from the kagome and mixed half and half strip, all combination lattice variations outperformed their single lattice counterpart. This was due to the form factor of two mechanically contrasting geometries within the same structure. The best lattice performance was from the kagome and half alternating unit cell strip at N = 20.

All cases exhibited a large frequency peak seen near the ring frequency of the structure. The introduction of low frequency cantilevers tuned to the ring frequency of the cylindrical shell was successful in trapping some of the energy from the ring mode. However, with the introduction of a 1.5 mm skin placed on the exterior of the lattice, this adversely affected the ability of the cantilevers to trap some of the ring mode energy. It was suspected that since the skin and cantilevers became coupled together upon implementation of the skin, the cantilevers were not allowed to displace as much which may have impeded the trapping of energy. Decoupling the cantilevers from the skin proved ineffective in suppressing this peak frequency. For future work, a joint resonator that is connected to the skin and the unit cell should be considered to suppress the dominant peak. Making the skin thinner seems to work, however, incorporating a resonator that connects both bodies may be effective in trapping the ring mode energy coming from the lattice and the skin of the structure. Furthermore, the inclusion of analyzing the strips in the frequency domain is also a potential next step. Instead of using a time-dependent approach, an initial frequency domain approach would allow for the evaluation of the different possible modes experienced by each lattice in the strip. Lastly, the inclusion of damping to our models is something that is yet to be explored.

APPENDIX

A. Single Strip Analysis

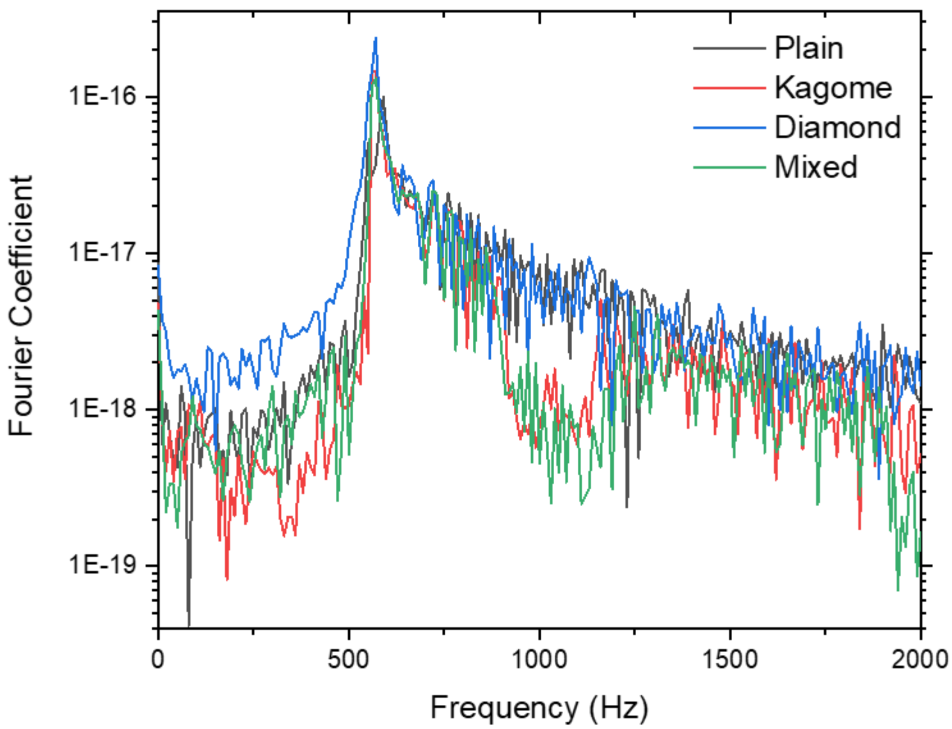

Figure A. 1: The frequency response for the out of plane displacement collected from the detector for the plain, kagome, diamond, and mixed strip at N = 12. A logarithm base 10 was implemented to the y-axis data for better illustration of each performance.

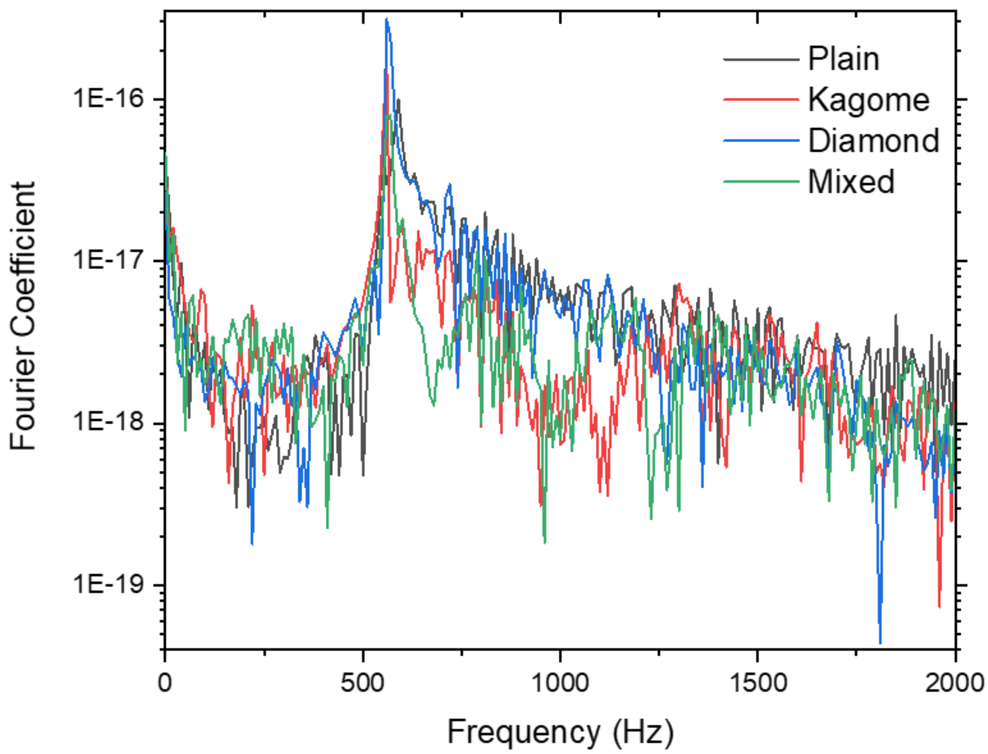

Figure A. 2: The frequency response for the out of plane displacement collected from the detector for the plain, kagome, diamond, and mixed strip at N = 36. A logarithm base 10 was implemented to the y-axis data for better illustration of each performance.

B. MATLAB Code

Fourier transform code used to convert the out of plane displacement data from the time domain to the frequency domain:

```
%% Fourier Transform

x=readmatrix('.txt'); % Out of Plane Displacement data from
time dependent simulation

t=x(:,1); % Time (s)
w=x(:,4); % Out of Plain Displacement (m)
q=isnan(t); t(q)=[]; w(q)=[];

 X=w; % Values to be transformed
 L=length(X);
 Y = fft(X.*hann(L)); TT=10^(-4); %hanning window added
```

```
Fs=1/TT;
P2 = abs(Y/L);
P1 = P2(1:L/2+1);
P1(2:end-1) = 2*P1(2:end-1);

f = Fs*(0:(L/2))/L;
figure
plot(f,P1)
title('Single-Sided Amplitude Spectrum of   X(t)')
xlabel('f (Hz)')
ylabel('|P1(f)|')
grid on
```

REFERENCES

[1] Maldovan M, Thomas EL, Periodic Materials and Interference Lithography for Photonics, Phononics and Mechanics, Wiley Interscience (2009)

[2] Gorishnyy, Taras, et al. “Sound Ideas.” Physics World, vol. 18, no. 12, Dec. 2005, pp. 24–29, doi:10.1088/2058-7058/18/12/30.

[3] Berg, Richard E. “Sound.” Encyclopædia Britannica, Encyclopædia Britannica, Inc., 20 Feb. 2020.

[4] Lucklum, R., and J. Li. “Phononic Crystals for Liquid Sensor Applications.” Measurement Science and Technology, vol. 20, no. 12, Dec. 2009, p. 12, doi:10.1088/0957-0233/20/12/124014.

[5] Deymier, Pierre A. Acoustic Metamaterials and Phononic Crystals. 1st ed. 2013., Springer Berlin Heidelberg, 2013, doi:10.1007/978-3-642-31232-8.

[6] Bourquin, Yannyk, et al. “Phononic Crystals for Shaping Fluids.” Advanced Materials, vol. 23, no. 12, WILEY-VCH Verlag, Mar. 2011, pp. 1458–62, doi:10.1002/adma.201004455.

[7] Wilson, Rab, et al. “Phononic Crystal Structures for Acoustically Driven Microfluidic Manipulations.” Lab on a Chip, vol. 11, no. 2, Jan. 2011, pp. 323–28, doi:10.1039/c0lc00234h.

[8] Hakoda, Christopher, et al. “Using Floquet Periodicity to Easily Calculate Dispersion Curves and Wave Structures of Homogeneous Waveguides”. 2018, doi:10.1063/1.5031513.

[9] COMSOL Multiphysics® Reference Manual, pp. 382-395. COMSOL Multiphysics® v. 5.5. COMSOL AB, Stockholm, Sweden. 2019

[10] Li-Yang Zheng. Granular monolayers: wave dynamics and topological properties. Acoustics [physics.class-ph]. Université du Maine, 2017. English. <NNT: 2017LEMA1035>. <tel-01654480>

[11] Lu, Ming-Hui, et al. “Phononic Crystals and Acoustic Metamaterials.” Materials Today (Kidlington, England), vol. 12, no. 12, Elsevier BV, 2009, pp. 34–42, doi:10.1016/s1369-7021(09)70315-3.

[12] Khelif, Abdelkrim, and Ali Adibi. Phononic Crystals: Fundamentals and Applications. 1st ed. 2016, Springer, 2016, doi:10.1007/978-1-4614-9393-8.

[13] Hussein, Mahmoud I., et al. “Dynamics of Phononic Materials and Structures: Historical Origins, Recent Progress, and Future Outlook.” Applied Mechanics Reviews, vol. 66, no. 4, July 2014, doi:10.1115/1.4026911.

[14] Brun, M., Movchan, A. B., and Jones, I. S., 2013, “Phononic Band Gap Systems in Structural Mechanics: Finite Slender Elastic Structures and Infinite Periodic Waveguides,” ASME J. Vib. Acoust., 135(4), p. 041013.10.1115/1.4023819

[15] Airoldi, L., and M. Ruzzene. “Design of Tunable Acoustic Metamaterials through Periodic Arrays of Resonant Shunted Piezos.” New Journal of Physics, vol. 13, no. 11, IOP Publishing, 2011, p. 113010–, doi:10.1088/1367-2630/13/11/113010.

[16] Koh, C. Y., 2011, “Generalized Phononic Networks: Of Length Scales, Symmetry Breaking and (Non) Locality: ‘Controlling Complexity through Simplicity.’” PhD Thesis, MIT (2011).

[17] Ni, S., 2014, “Phononic Metamaterials Based on Complex Geometries "A New Kind of Metamaterial"” PhD Thesis, MIT (2014).

[18] Wagner, Markus R., et al. “Two-Dimensional Phononic Crystals: Disorder Matters.” Nano Letters, vol. 16, no. 9, American Chemical Society, Sept. 2016, pp. 5661–68, doi:10.1021/acs.nanolett.6b02305.

[19] Bao, Jing, et al. “Dynamic Responses of a Structure with Periodic Foundations.” Journal of Engineering Mechanics, vol. 138, no. 7, American Society of Civil Engineers, July 2012, pp. 761–69, doi:10.1061/(ASCE)EM.1943-7889.0000383.

[20] Airoldi, L., and M. Ruzzene. “Design of Tunable Acoustic Metamaterials through Periodic Arrays of Resonant Shunted Piezos.” New Journal of Physics, vol. 13, no. 11, IOP Publishing, 2011, p. 113010–, doi:10.1088/1367-2630/13/11/113010.